

Synthesis, biological activity, DNA binding and anion sensors, molecular structure and quantum chemical studies of a novel bidentate Schiff base derived from 3,5-bis(trifluoromethyl)aniline and salicylaldehyde

Mustafa Yıldız^{a,b*}, Özge Karpuz^a, Celal Tuğrul Zeyrek^c, Bahadır Boyacıoğlu^d, Hakan Dal^e, Neslihan Demir^f, Nuray Yıldırım^g, Hüseyin Ünver^{h*}

^aDepartment of Chemistry, Faculty of Arts and Sciences, Çanakkale Onsekiz Mart University, TR-17100 Çanakkale, Turkey.

^bNanoscience and Technology Research and Application Center (NANORAC), Çanakkale Onsekiz Mart University, Çanakkale, Turkey

^cAnkara Nuclear Research and Training Center, Turkish Atomic Energy Authority, TR-06100 Besevler-Ankara, Turkey

^dVocational School of Health Services, Ankara University, TR-06290 Kecioren-Ankara, Turkey

^eDepartment of Chemistry, Faculty of Science, Anadolu University, TR-26470 Yenibağlar, Eskişehir, Turkey

^fDepartment of Biology, Faculty of Arts and Sciences, Çanakkale Onsekiz Mart University, TR-17100 Çanakkale, Turkey.

^gHealth Services Vocational School, Çanakkale Onsekiz Mart University, TR-17100 Çanakkale, Turkey

^hDepartment of Physics, Faculty of Science, Ankara University, TR-06100 Besevler-Ankara, Turkey

E-mail:myildiz@comu.edu.tr (Mustafa Yıldız)
unverh@ankara.edu.tr (Hüseyin Ünver)

ABSTRACT

Synthesis, biological activity, spectroscopic and crystallographic characterization and density functional theory (DFT) studies of the Schiff base 3,5-bis(trifluoromethyl)aniline and salicylaldehyde are reported. It crystallizes as a monoclinic space group $P2_1/c$ with $a=7.7814(3)\text{Å}$, $b=26.8674(9)\text{Å}$, $c=7.4520(2)\text{Å}$, $V=1379.98(8)$, $Z=4$, $D_c=1.6038\text{ g cm}^{-3}$, and $\mu=0.156\text{ mm}^{-1}$. The molecular structure obtained from X-ray single-crystal analysis of the investigated compound in the ground state was compared using Hartree-Fock (HF) and density functional theory (DFT) with the functionals B3LYP and B1B95 using the 6-311++G(d,p) basis set. The antimicrobial activities of the compound were investigated for its minimum inhibitory concentration (MIC). The interaction of the Schiff base with calf thymus DNA was investigated using UV-visible spectra. The colorimetric response of the Schiff base

receptors in DMSO was investigated before and after the addition of an equivalent amount of each anion to evaluate the anion recognition properties.

Keywords: Schiff base; Density functional theory; Antimicrobial activity; Tautomerism; Calf thymus-DNA; Anion sensors.

1. Introduction

Schiff bases have been reported for their biological properties, such as antibacterial, antifungal, antiinflammatory, analgesic, anticonvulsant, antitubercular, anticancer, antioxidant and antihelmintic activities [1-26]. Schiff base metal complexes have applications in the areas from material science to biological sciences. They have been widely studied because they have anticancer and herbicidal applications [20-21]. Schiff base complexes show greater biological activity than free ligands [3, 6, 22-26]. The DNA binding, cytotoxicity and apoptosis induction activity were studied for Schiff base copper(II) complexes [27-29]. A rather commonly used technique regards the development of fluorescent chemosensor quenching of fluorescence by interaction with anions. The sensors can provide fast and visible color changes from yellow to red in the presence of strong basic anions. Over the past 10 years, several excellent chemosensors have been reported for recognition and sensing of anions with high selectivity and sensitivity [30-37]. Tautomerism in Schiff bases with an OH group in ortho position to the imino group both in solution and in solid state were investigated using spectroscopy and X-ray crystallography techniques [4-5, 38-44]. Schiff bases with OH group in ortho position to the imino group are of interest mainly due to the existence of either O-H \cdots N or O \cdots H-N type hydrogen bonds and tautomerism between enol-imine and keto-amine form. In some instances the hydrogen from the OH group is completely transferred to the imine nitrogen. In other words, enol-imine \rightleftharpoons keto-amine equilibrium shifts

predominantly to the keto-amine side. The keto-amine form is always observed when the Schiff base is derived from 2-hydroxy-1-naphthaldehyde and aromatic amine. In Schiff bases derived from salicylaldehyde and aromatic amines, the keto-amine form is not observed in solution and solid state.

In this study, a novel bidentate Schiff base has been synthesized by the reaction of 3,5-bis(trifluoromethyl)aniline with 2-hydroxy-1-benzaldehyde. The structure of the synthesized Schiff base was investigated using data obtained from elementary analysis, FT-IR, UV-visible, $^1\text{H-NMR}$ and $^{13}\text{C-NMR}$ techniques. The solid state structure of the Schiff base (*E*)-2-[(3,5-bis(trifluoromethyl)phenylimino)methyl]phenol (Scheme 1) was also determined crystallographically. The minimal inhibitory concentration (MIC) of the compound was screened in vitro against bacteria and yeast cultures using broth micro dilution tests [45-48]. DNA binding of the Schiff base was investigated. Also, anion sensing ability of the Schiff base was observed colorimetrically in DMSO for F^- , Br^- , I^- , CN^- , SCN^- , ClO_4^- , HSO_4^- , CH_3COO^- , H_2PO_4^- , N_3^- and OH^- anions. The molecular structure, atomic charges, molecular electrostatic potential (MEP), nonlinear optical (NLO) effects and thermodynamic properties of the compound were investigated by DFT. The result of theoretical calculations was compared with crystallographic data. Additionally, we theoretically investigated the geometric structure and energy contents of both enol-imine and keto-amine tautomers of the compound.

2. Experimental

2.1. Reagents and techniques

The ^1H and ^{13}C NMR spectra were recorded on a Bruker AVANCE- 500 spectrometer operating at 400 and 101,6 MHz. Infrared absorption spectra were obtained from a Perkin Elmer BX II spectrometer in KBr discs and were reported in cm^{-1} units. The UV-VIS spectra were measured using a SHIMADZU 1800 series spectrometer. Elementary analyses were

performed on a Vario EL III CHNS elemental analyzer. Melting points were measured with an Electro Thermal IA 9100 apparatus using a capillary tube. 3,5-Bis(trifluoromethyl)aniline, salicylaldehyde, EtOH, Ethidium bromide (EB), calf thymus DNA (CT-DNA), (Bu)₄NF, (Bu)₄NBr, (Bu)₄NI, (Bu)₄NCN, (Bu)₄NSCN, (Bu)₄NCIO₄, (Bu)₄NHSO₄, (Bu)₄NCH₃COO, (Bu)₄NH₂PO₄, (Bu)₄NN₃, (Bu)₄NOH and DMSO were purchased from Aldrich. The Tris–HCl buffer solution was prepared with triple-distilled water. CT-DNA stock solution was prepared by diluting DNA to Tris–HCl/NaCl buffer (5 mM Tris–HCl, 50 mM NaCl, pH 7.2), and kept at 4 °C for no longer than two days.

2.2. Synthesis of (*E*)-2-[(3,5-bis(trifluoromethyl)phenylimino)methyl]phenol

3,5-Bis(trifluoromethyl)aniline (0.50 g, 2.18x10⁻³ mol) was added to EtOH (100 mL) solution of salicylaldehyde (0.265 g, 2.18x10⁻³ mol) [44]. The mixture was stirred and refluxed for 1 h. Compound (**1**) was obtained from the evaporation of EtOH. It was crystallized from CHCl₃ : n-hexane (3:2) as a yellow crystal, mp 86 °C, 0.57 g (85%) yield. Found: C, 54.05; H, 2.72; N, 4.20. Calc. For C₁₅H₉F₆NO; C, 54.07; H, 2.70; N, 4.20 %. IR(KBr, cm⁻¹); νO-H; 3434 m, νAr-H; 3098 w, νC=N; 1629 s, νC=C; 1616-1602, 1582s, νC-N; 1497 m, νC-O; 1361m. ¹H-NMR (DMSO); δ ppm, 12.25 (s, 1H, Ar-OH); 9.07 (s, 1H, Ar-CH=N-); 8.10-6.97 (m, 7H, Ar-H). ¹³C-NMR (DMSO); δ ppm, 119.89 (s, 1C, C-CH=N); 160.23 (s, 1C, C-OH); 116.73 (s, 1C, CH-C-OH); 132.71 (s, 1C, CH-CH-C-OH); 122.07 (s, 1C, CH-CH-C-CH=N); 131.48 (s, 1C, CH-C-CH=N); 166.57 (s, 1C, -CH=N); 150.62 (s, 1C, C-N=CH); 124.24 (s, 2C, CH-C-N=CH); 134.15 (s, 2C, C-CF₃); 122.48 (s, 1C, CH-C-CF₃); 131.21 (s, 2C, CF₃).

2.3. Crystallography

Crystallographic data were recorded on a Bruker Kappa APEXII CCD area-detector diffractometer using MoK_α radiation (λ = 0.71073Å) at T = 100 K. Data collection, reduction and corrections for absorption and crystal decomposition for the compound were achieved by

using X-Area, X-RED software [49] and the structure was solved by SHELXS-97 and refined with SHELXL-97 [50-51]. The positions of the H atoms bonded to C atoms were calculated (C-H distance 0.96 Å), and refined using a riding model, but the H1 atom of the O1 was found in a difference electron-density map at the end of the refinement process as a small positive electron density. All atoms (except hydrogen) were located from a difference Fourier map and refined anisotropically. The atoms of C(10)F₃ group are disordered over two positions. For F1, F2 and F3 atoms the site occupancy factor is 0.65 and for F1A, F2A, and F3A atoms the site occupancy factor is 0.35. The details of the X-ray data collection, structure solution and structure refinements are given in Table S1. The bond distances, bond and torsion angles are listed in Table S2. The molecular structure with the atom-numbering Scheme is shown in Fig.1 [52]. Crystallographic data (excluding structure factors) for the structures reported in this paper has been deposited with the Cambridge Crystallographic Data Centre as supplementary publication number CCDC 1038662 [53].

2.4. Screening for antimicrobial activities

Bacillus subtilis ATCC 6633, *Saphylococcus aureus* ATCC 25923, *Escherichia coli* ATCC 25922, *Enterococcus faecalis* ATCC 29212, *Pseudomonas aeruginosa* ATCC 254992, *Escherichia coli* ATCC 35218, *Bacillus cereus* NRRL B-3711, *Proteus vulgaris* ATCC 13315, *Candida albicans* ATCC 60193, and *Candida tropicalis* ATCC 13803 were used as microorganisms. Gentamicin, ampicillin and fluconazol were used as controls in this study as they are well-known broad-spectrum antibiotics that have different mechanisms of activity, such as interruption of protein synthesis (gentamicin) and inhibition of cell wall synthesis (ampicillin) [54]. The compounds were dissolved in DMSO (dimethyl sulfoxide) to a final concentration of 500 µg/mL. The concentration of the compounds on different plates was 500 µg/mL, 250 µg/mL, 125 µg/mL, 62.5 µg/mL, 31.25 µg/mL, 15.6 µg/mL, 8 µg/mL, 4 µg/mL, 2 µg/mL, and 1 µg/mL.

2.5. DNA-Binding experiments

The UV-visible spectra titrations were carried out in Tris-HCl/NaCl buffer at room temperature to investigate the binding affinity between CT-DNA and the Schiff base. The UV-VIS absorbance at 260 and 280 nm of CT-DNA solution in Tris buffer give a ratio of 1.8–1.9, indicating that the DNA was sufficiently free of protein [55]. Tris-HCl/NaCl buffer (3 mL) and the solutions of Schiff base (3 mL, 1.13×10^{-5} M) were placed into two cuvettes, respectively. Then one aliquot (5 μ L, 0.01 M) of buffered CT-DNA solution was added to each cuvette in order to eliminate the absorbance of DNA itself. Before the absorption spectra were recorded, the Schiff base-DNA solutions were incubated at room temperature for 5 min.

2.6. Anion Sensors Measurements

Schiff base (0.05 μ mol) was dissolved in DMSO (50 mL). Tetrabutylammonium salts (F^- , Br^- , I^- , CN^- , SCN^- , ClO_4^- , HSO_4^- , CH_3COO^- , $H_2PO_4^-$, N_3^- , OH^-) (0.05 μ mol) were dissolved in DMSO (50 mL). Each solution of tetrabutylammonium salts was added to the Schiff base solution (1:1) in the UV tube. After mixing them, UV absorption spectra were taken at room temperature.

2.7. NMR Titration

Three NMR tubes of Schiff base dissolved in DMSO- d_6 were prepared and then different equivalents (0.0, 0.5, and 1.0 equiv.) of tetraethylammonium fluoride dissolved in DMSO- d_6 were added to two solution of Schiff base tube. After shaking thoroughly, 1H NMR spectra were taken at room temperature.

2.8. Calculation details

The molecular geometry of the compound was taken directly from the X-ray diffraction experimental result of the geometry optimization. This result was used in the Gaussian 09W software package and the Gauss-view visualization program [56-57] for DFT calculations with Becke's one and three-parameter hybrid exchange functionals (B1 and B3)

[58-59] using Becke's time-dependent gradient-corrected (B95) [58] and Lee-Yang-Parr (LYP) correlation functionals with the 6-31G(d), 6-31+G(d,p), 6-31++G(d,p), 6-311+G(d) and 6-311++G(d,p) basis sets [60-63].

It is well-known that the vibrational wavenumbers obtained by DFT computations are usually overestimated compared to their experimental counterparts. To overcome discrepancies between observed and calculated wavenumbers, the scaling factors have been introduced by using the relationship between the calculated unscaled (ν_{ucal}) and experimental (ν_{exp}) wavenumbers is linear and is described by the following equation:

$$\nu_{exp} = 0.97964\nu_{ucal} - 23.43068, \quad R^2 = 0.99639 \quad (1)$$

According to the fitting results of equation (1), the general scale factor value was found to be 0.97964 for B3LYP/6-311++G(d,p) level. We calibrated the vibrational wavenumbers by using a scale factor value of 0.97964. The assignments of each vibrational mode were defined from their potential energy distributions (PED) which were calculated by using VEDA 4 program based on B3LYP [64]. The visual checks for the vibrational band assignments were also performed by using Gauss-View molecular visualization program.

To investigate the tautomeric stability, some properties such as total energy, HOMO and LUMO energies of the compound in gas phase were obtained at B3LYP/6-311++G(d,p) level. These properties were also examined in five kinds of solvent media (chloroform, dichloroethane, ethanol, dimethylsulfoxide and water) by using a Polarized Continuum (PCM) model. To investigate the reactive sites and to identify sites of intra- and intermolecular interactions of the compound, the molecular electrostatic potential surface was evaluated by using B3LYP/6-311++G(d,p) method. The total molecular dipole moment (μ), linear polarizability (α), and the first-order hyperpolarizability (β) was predicted by the B3LYP method with different base sets, 6-31G(d), 6-31+G(d,p), 6-31++G(d,p), 6-311+G(d) and 6-311++G(d,p), to investigate the effects of basis sets on the NLO properties.

Finally, the standard thermodynamic functions were obtained from statistical thermodynamics based on the vibrational frequency analysis at B3LYP/6-311++G(d,p) level using the Gaussian 09 software package.

3. Results and discussion

3.1. Crystallographic study

2-Hydroxybenzaldehyde Schiff base ligands are of interest mainly due to the existence of either O \cdots H – N or O – H \cdots N type hydrogen bonds and the tautomerism between enol and keto forms [65-66]. The crystal structure is stabilized by intramolecular and intermolecular hydrogen bonding of these types of ligands [65-66]. In the compound, hydrogen bonds are observed between the 2-hydroxy group and the imine nitrogen atom. In some instances, the hydrogen atom from the phenol group is completely transferred to the imine nitrogen atom or is just converse. In the Schiff base ligand studied in this paper, the molecule is not planar in the solid state. **A** [O1, C1-C7] and **B** [N1, C8-C15, F1-F6] are inclined at an angle of 29.30 (8) $^\circ$. In the crystal structure of the compound there is a strong intramolecular O \cdots H–N hydrogen bond [O1–H1 = 0.804 Å, H1 \cdots N1 = 1.942 Å, O1 \cdots N1 = 2.608(3) Å]. The sum of the Van der Waals radius of the O and N atoms (3.07 Å) is significantly longer than the intramolecular O \cdots N hydrogen bond length [67]. This intramolecular hydrogen bond can be compared with *N*-[2-hydroxy-1-naphthylidene]3,5-bis(trifluoromethyl)aniline 2.558(7) Å [44].

In the compound, the C=N group seems to have a strong electron withdrawing character. Thus, the O1-C1 bond distance of 1.359(5) Å is also consistent with the C-O single bonding; similarly the C7=N1 distance of 1.290(5) Å is a consistent with the C=N double bonding. For these bonds, when we compare with our previous work [44], C-O 1.327(8) Å is longer and C=N 1.308(7) Å is shorter. In addition to spectroscopic studies, the existence of the enol-imine tautomer was also confirmed by using X-ray diffraction data.

3.2. Optimized molecular structure

The molecular structure of (*E*)-2-[(3,5-bis(trifluoromethyl)phenylimino)methyl]phenol was experimentally determined. Geometric optimization of the compound was performed by using DFT/B3LYP method with 6-311++G(d,p) basis set (Table S2). The calculated bond distances, bond angles and torsion angles are compared with the experimental values for the compound, and are shown in Fig. S2a, b, c. The aniline ring is rotated relatively to the salicylaldimino part in both the optimized and experimental structures.

The conformational discrepancies between the X-ray structure and optimized counterparts can be seen from Fig. S2a, S2b, S2c. According to Fig. S2a and S2b, the biggest difference in bond lengths between the experimental and the optimized values is found for the C14–F2 bond with the difference being 0.1075 Å, and the biggest difference for the bond angles is found as 5.53° at F2–C14–F3. The discrepancy for the enol form is less than for the keto form, as seen in Fig. S2a and S2b. The orientation of CF₃ groups is a remarkable discrepancy between these counterparts and the orientation of these groups is defined by torsion angles C9–C10–C14–F2, C11–C12–C15–F6, C9–C10–C14–F3 and C11–C10–C14–F1 with values of 1.1(7)°, -80.1(5)°, 115.7(5)° and 53.1(6)° from X-ray, respectively. The differences in the torsion angles between the experimental and calculated values are 59.52° (C11–C12–C15–F6) for HF, 18.34° (C9–C10–C14–F2) for the B3LYP and 29.15° (C9–C10–C14–F3) for B1B95. In the structure of the Schiff base molecule, the most important torsion angles between the aniline ring with the salicylaldimino-part are [θ_1 (C8–N1–C7–C6)], [θ_2 (C7–N1–C8–C13)] and [θ_3 (C5–C6–C7–N1)]. From the X-ray structure determination, [θ_1 (C8–N1–C7–C6)], [θ_2 (C7–N1–C8–C13)] and [θ_3 (C5–C6–C7–N1)] values were obtained as 177.1(3)°, -32.7(5)° and -178.1(4)°, respectively. These angles have been calculated as 176.99°, -39.77° and -179.11° for B3LYP/6-311++G(d,p); 178.33°, -46.46° and -178.91° for HF/6-311++G(d,p); and 177.62°, -38.52° and -179.08° for the B1B95/6-311++G(d,p) level in

the optimized structure in Table S2 and Fig. S2c. As seen from Table S2, most of the optimized bond lengths are slightly longer than the experimental values. It can be said that the experimental results belong to the solid phase, whereas the theoretical calculations belong to the gas-phase. The resulting differences of bond parameters between the calculated and experimental values depend on the existence of the crystal field along with the inter-molecular interactions connecting the molecules together in the solid state. The geometric parameters calculated using the B3LYP/6-311++G(d,p) method are in good agreement with the X-ray structure.

According to these results, it may be concluded that the HF/DFT(B3LYP-B1B95) calculations well reproduce the bond distances and the bond angles for the enol-imine form, while the same calculations are better at predicting the torsion angles for the keto-amine form of the compound.

In spite of the small differences, calculated geometric parameters represent a good approximation, and they are the basis for calculating other parameters such as PES scan, vibrational frequencies, atomic charges, molecular electrostatic potential (MEP), nonlinear optical (NLO) effects and thermodynamic properties of the compound, as described below.

3.3. Potential energy surface (PES) scan

To investigate the conformational stability of the compound, the potential energy surface (PES) scans for the link fragments of the aldehyde ring (ring1) with respect to the aniline ring (ring2) part in the whole molecule were investigated. For this reason, the torsion angles $T1(C9-C8-N1-C7)$ and $T2(C1-C6-C7-N1)$ are relevant coordinates for conformational flexibility of the investigated molecule. The scans were obtained by minimizing the potential energy using B3LYP/6-311++G(d,p) level of theory in all geometrical parameters by varying the torsion angles in steps of 10° in the range of $0-360^\circ$

rotation around the bond. The variations of potential energy change from its equilibrium with the torsional perturbation are presented in Fig. S3a and S3b.

Potential energy surface (PES) scan for torsion angle T1 showed three minima positions at 70° , 170° and 250° , while T2 shows one minimum position at 170° . Among these, the deepest minima values correspond to the optimized molecular geometry [T1(C9–C8–N1–C7) = 250° and T2(C1–C6–C7–N1) = 170°] of the compound which is directly taken from the X-ray diffraction experimental result. The energy of the most stable conformation is -306.45009680 Hartree.

3.4. Vibrational spectra

The infrared spectra of the investigated compound were recorded in the $4000\text{--}400\text{ cm}^{-1}$ region using KBr pellets on a Perkin Elmer BX II spectrometer and are given in Fig. 4. The vibrational band assignments were performed at B3LYP/6-311++G(d,p) theory level to compare the experimental (FT-IR) and calculated vibrational frequencies of the compound. We analyzed the normal vibrational frequencies and compared our calculated results for the investigated compound with the experimental ones on the basis of potential energy distributions (PED), given in Table S3. The infrared spectra of the investigated compound have some characteristic bands for stretching vibrations of the O–H, C–H, C = N, C–O, C–C, and C–F₃ groups.

3.4.1. Hydroxyl group vibrations

The characteristic region of the O–H group vibration spectrum in the Schiff bases, which have a free hydroxyl group or non-hydrogen bonded, is $3550\text{--}3700\text{ cm}^{-1}$ [68]. If the intramolecular hydrogen bonding occurs in six membered ring systems, the O–H stretching band will be reduced to the $3550\text{--}3200$ region [69]. In this study, the experimental O–H stretching vibration was observed at 3434 cm^{-1} . The O–H stretching vibration was calculated as 3225 cm^{-1} for B3LYP/6-311++G(d,p) level with 99% contribution of PED. The

experimentally and theoretically predicted frequency for O–H vibration by B3LYP/6-311++G(d,p) level shows excellent agreement with the recorded spectrum, as well as the literature data, and is also supported by PED values [70-72]. The strong hydrogen bonding if present in the Schiff bases composed of the 2-hydroxy-1-naphthaldehyde system would reduce the O–H stretching band shifting to a lower wavenumber 2900 cm^{-1} [73]. In plane O–H bending modes are observed at 1533, 1467, and 1381 cm^{-1} , while the corresponding bands are calculated at 1573, 1496, and 1448 cm^{-1} with 14%, 19%, and 41% contribution of PED. The band observed at 846 cm^{-1} is assigned as an out of plane bending of the O–H group, and this band is calculated at 855 and 807 cm^{-1} for B3LYP with 13% and 23% contribution of PED, respectively.

3.4.2. C–H vibrations

The aromatic structure shows the presence of C–H stretching vibrations in the region $3000 - 3125\text{ cm}^{-1}$, which is the characteristic region for the identification of $\nu(\text{CH})$ stretching vibrations. But in this region, the bands are not appreciably affected by the nature of the substituent [74]. In the FT-IR spectrum of the compound, symmetric C–H stretching vibrations are observed at 3067 and 3098 cm^{-1} . The corresponding bands are calculated at 3135 and $3151/3145\text{ cm}^{-1}$ with 99% and 99/100% contribution of PED. The observed asymmetric C–H stretching vibration is 2990 cm^{-1} , while the calculated values for the asymmetric C–H stretching vibrations are $3129/3108/3097\text{ cm}^{-1}$ with 98/36/65% contribution of PED. Substitution sensitive C–H in-plane bending vibrations lie in the region $1000-1300\text{ cm}^{-1}$ [71]. In the compound, infrared bands ranging from 1240 and 1133 cm^{-1} are assigned to C–H in-plane bending vibrations. These vibrations correspond to 1268 and 1155 cm^{-1} from the calculated values. The C–H out-of-plane bending vibrations appear in the range $1000-675\text{ cm}^{-1}$ [71, 75-76]. The observed vibrations are 950, 900, 858, 846 and 735 cm^{-1} for the C–H out-of-plane bending vibrations. The bands at 973, 907/897, 884, 855, and 751 cm^{-1} are

assigned to the C–H out-of-plane bending vibrations for the investigated compound. As seen in Table S3, the C–H out-of-plane bending vibrations are assigned as mixed and pure modes, respectively.

3.4.3. C=N vibrations

The C=N stretching vibrations were assigned in the region 1500-1600 cm^{-1} by Silverstein [77]. In the present study, the C=N bond stretching vibration band is observed at 1602 experimentally, while it is calculated at 1632/1627 cm^{-1} with B3LYP/6-311++G(d,p) level. The PED for this mode is 16 and 31%. The PED for this mode suggests that this is a mixed mode (Table S3). The band at 1170 cm^{-1} is designated as C–N stretching vibration, and this mode is assigned at 1178 cm^{-1} by B3LYP level. For C=N and C–N stretching vibrations, the results observed and calculated by B3LYP/6-311++G(d,p) method are in good agreement with similar Schiff base compounds [70, 73, 78].

3.4.4. Phenyl ring vibrations

The ring C=C stretching vibrations for the aromatic group generally appear at 1430-1625 cm^{-1} [79]. For this compound, the C=C stretching vibrations are observed at 1602, 1582, 1561, 1533, and 1400 cm^{-1} in FT-IR spectrum. These vibrations correspond to 1632/1627, 1601, 1573, and 1448 from the calculated values. The bands at 1332, 1319, 1268, and 1235 cm^{-1} are also assigned to C–C stretching vibrations for the investigated compound. These vibration modes are highly mixed modes with the range of 11-58% contribution of PED. The mean difference between the theoretical and experimental frequencies is about 14 cm^{-1} . It shows good agreement between theoretical and experimental values of the ring C=C and C–C stretching vibrations for the aromatic group.

3.4.5. C–O and C–F vibrations

The C–O stretching vibrations appear in the spectral range 1168-1310 [80]. For the compound, the phenolic C–OH stretching vibration is observed at 1278 cm^{-1} and assigned at

1291 cm^{-1} with 38% contribution of PED. For C–OH stretching vibration, the result observed and calculated by B3LYP/6-311++G(d,p) method are in good agreement with similar Schiff base compounds [70, 73, 78]. The bands at 1120 and 1030 cm^{-1} in the FT-IR spectrum are appointed as C–F stretching vibrations and these modes are calculated in the range of 660–1230 cm^{-1} . According to the calculations 1140 and 717 cm^{-1} are assigned to the symmetric C–F₃ stretching modes, while the 1132 cm^{-1} vibration is the asymmetric C–F₃ stretching mode. In the predicted spectra, out-of plane F–C–F bending vibration is appointed at 656 cm^{-1} with 31% contributions of PED.

The calculated values of other group vibrations show good agreement with the experimental results. The other experimental and calculated vibrational values can be seen in Table S3. To make a comparison with the experimental observations, we present correlation graphics in Fig. S5a and S5b. The relationships between experimental (ν_{exp}) and calculated scaled (ν_{cal}) wavenumbers is linear and described by the following equation:

$$\nu_{exp} = 1.00332\nu_{cal} - 26.75329 \quad R^2 = 0.9976 \quad (2)$$

As a result, the scaled fundamental vibrationals have good consistency with experimental results and are found in good agreement with that predicted in the literature.

3.5. ¹H NMR and ¹³C NMR Spectroscopic studies

The ¹H-NMR and ¹³C-NMR data are given in synthetic procedures for the compound. The ¹H-NMR data for the compound show that the tautomeric equilibrium favours the enol-imine in DMSO. The -OH and -CH=N- protons are observed at 12.25 and 9.07 ppm singlets for the compound (Table 4). The phenyl protons of the compound gave multiplets at 8.10–6.97 ppm. According to the ¹³C-NMR spectra, the compound has 12 signals, showing that the structures in solution are symmetrical (Fig. S6).

In nuclear magnetic resonance spectroscopy (NMR) the isotropic chemical shift analysis allows us to identify relative ionic species and to calculate reliable magnetic

properties which provide accurate predictions of molecular geometries [50-53]. The optimized molecular geometry of the compound was obtained by using the B3LYP method with 6-311++G(d,p) basis set in gas phase and DMSO solvent with the IEFPCM solvent model. Then, the proton and carbon-13 NMR chemical shifts were calculated at the same level by using the GIAO method. The calculated and experimental ^1H - and ^{13}C -NMR chemical shift values for the Schiff base molecule are listed in Table 4. As seen from Table 4, the hydrogen atoms in the hydroxyl and imine groups have resonance in the range 12.33-8.95 ppm [81]. The H(-O) and H7 atoms in hydroxyl and imine groups of the molecule produced a resonance signal at 12.25 and 9.07 ppm. The calculated values for these hydrogen atoms are 12.26/8.61 ppm (in the gas phase) and 12.33/8.84 ppm (in DMSO), respectively. The protons in phenol groups give rise to a signal in the interval 4-7.5 ppm, depending on concentration, solvent and temperature [81]. But the phenolic proton under intra-intermolecular hydrogen bonding interaction gives a resonance signal between 10–12 ppm [81]. The observed resonance signals between 6.97–8.10 ppm correspond to chemical shifts of the protons in the aromatic rings. The calculated chemical shifts for aromatic protons are calculated (in the gas phase/DMSO) as 6.95/7.90 and 7.14/7.96 ppm, respectively.

The carbon-13 NMR chemical shift values in aromatic rings and carbon atoms which are bonded to electronegative F, O and N atoms are observed at the interval 116.73–166.57 ppm. The chemical shifts of the C2 and C7 carbon atoms which are bonded to O and N atoms in hydroxyl and imine groups are observed at 160.23 and 166.57 ppm, respectively. Similarly, the chemical shifts of the C8, and C14/C15 atoms which are bonded to one N and F atom are observed at 150.62 and 131.21/ ppm. The calculated values for the C2, C7, C8 and C14/C15 atoms are (in gas phase/DMSO) 170.71/169.48, 169.64/172.07, 158.00/158.16, and 133.19/133.58, 133.24/133.69 ppm, respectively. For aromatic carbons, the experimental and

calculated ^{13}C NMR chemical shifts are between 166.57–116.73 ppm and 169.64–122.31/172.07–121.14 ppm (in gas phase/DMSO), respectively.

3.6. UV-Visible and HOMO–LUMO analysis

The UV-VIS spectrum of the compound was studied in DMSO (Fig. S7). The Schiff bases show absorption in the range greater than 400 nm in polar and nonpolar solvents. It should be pointed out that the new band belongs to the keto-amine form of the Schiff base with -OH group in ortho position to the imino group in polar and nonpolar solvents in both acidic and basic media [38-39]. The band was not observed at greater than 400 nm in DMSO for the compound. The enol-imine form is dominant in DMSO for the compound. The experimental UV-vis spectrum of the compound shows only two broad bands at 279 nm and 342 nm, which are assigned to the $\pi-\pi^*$ and $n-\pi^*$ transition of C=C and C=N. The computed UV-Vis was processed using the TD-DFT method on the B3LYP and 6-311G(d,p) basis set in Gaussian 09W software package [56]. The main results of experimental and TD-DFT calculated absorptions are summarized in Table S5. In DMSO solvent, the experimental spectrum presents two maximum absorption bands between 279 and 342 nm, whereas the TD-DFT results predict these bands around 290 and 345 nm. Experimentally, the long-wavelength maximum shifts towards high energy when the solvent polarity is increased, in agreement with previous reports [73, 78]. Comparing the experimental and the TD-DFT results shown in Table S5, a reasonable concordance between the wavelengths is observed. In addition, the UV absorption band at 346 nm of the compound results from an electronic transition from HOMO to LUMO localized mainly on the aromatic ring $\pi-\pi^*$ transition of the C=C from experimental results.

There are the other two absorption bands located at 306 and 290 nm, arising from HOMO-1 LUMO and HOMO LUMO+1 transitions which were estimated as $\pi-\pi^*$ and $n-\pi^*$ transition of the C=C and C=N transitions as seen in Table S5 and Fig. S8. Because the band

was not observed at greater than 400 nm in DMSO for the compound, in the keto form the HOMO-LUMO transition has not been observed at higher wavelengths because the energy of HOMO in keto structure is higher than that in enol structure and the energy of LUMO in the keto structure is lower than that in enol structure. The most important orbitals in a molecule are the frontier molecular orbitals, called HOMO and LUMO. These orbitals determine the way the molecule interacts with other species. The frontier orbital gap helps characterize the chemical reactivity and kinetic stability of the molecule. A molecule with a small frontier orbital gap is more polarizable and is generally associated with a high chemical reactivity, low kinetic stability and is also termed a soft molecule [82]. The energy gap between HOMO and LUMO is a critical parameter to determine molecular electrical transport properties. By using HOMO and LUMO energy values for a molecule, chemical hardness–softness, electronegativity and electrophilicity index can be calculated as follows:

$$\eta = \frac{1}{2}(I - A) \quad (3)$$

In equation (3) I is the vertical ionization energy and A stands for the vertical electron affinity. According to the Koopman theorem [83], the ionization energy and electron affinity can be equalized through HOMO and LUMO orbital energies:

$$EA = -\varepsilon_{HOMO} \quad (4)$$

$$IP = -\varepsilon_{LUMO} \quad (5)$$

According to the equation (4), the hardness corresponds to the gap between the HOMO and LUMO orbitals. Hence, the larger the HOMO-LUMO energy gap, the harder molecule.

$$\eta = \frac{1}{2}(\varepsilon_{LUMO} - \varepsilon_{HOMO}) \quad (6)$$

For enol and keto forms of the compound, the chemical hardness (η) was calculated with the B3LYP/6-311++G(d,p) base set. The results are given in Table S6. The energy separation between the HOMO and LUMO is 4.039 eV for the enol form and 3.179 eV for the

keto form. This large HOMO–LUMO gap for the enol form suggests high excitation energies for many of the excited states, a good stability and high chemical hardness for the compound. Indeed, as seen from Table S6 the chemical hardness of the enol form ($\eta_{enol}= 2.0195$ eV) is greater than the keto one ($\eta_{keto}= 1.5894$ eV), which once again indicates that the enol form of the molecule is more stable than its keto form in the gas phase, respectively.

3.7. Atomic charge distributions, energy and dipole moment behavior in the gas and the solution phases

The Mulliken atomic charges for the excluded H atoms of the compound have been calculated at B3LYP and B1B95/6-311++G(d,p) level using the Self-Consistent Isodensity Polarized Continuum Model (SCI-PCM) in the gas phase (Fig. S9). In order to investigate the solvent effect, five kinds of solvent were selected ($\epsilon= 4.9$, chloroform; $\epsilon= 10.36$, dichloroethane; $\epsilon= 24.55$, ethanol; $\epsilon= 46.7$, dimethylsulfoxide and $\epsilon= 78.39$ water) and the atomic charge distributions of the compound were also calculated using density functional theory (DFT) with the functional B3LYP 6-311++G(d,p) basis set. The calculated values for atomic charges of the compound in the gas phase and solution phase are listed in Table S7. According to the calculated Mulliken atomic charges, the imine N1 atom has a positive atomic charge and hydroxyl O1 atom has a large negative atomic charge in the gas phase. This behavior may be the result of the N1–H \cdots O1 hydrogen bond. On the other hand, as shown in Table S7, the negative atomic charge values of the O atom in solution phase become more negative while the positive atomic charge of N1 decreases with the increase in the polarity of the solvent.

The total energies and dipole moments of the compound were also calculated with B3LYP/6-311++G(d,p) level for five solvents in order to evaluate the difference in total energy and dipole moment behavior of the compound in solvent media. The results are given

in Table S8. According to the results, the obtained total energy of the compound decreases with the increasing polarity of the solvent. We can conclude that the stability of the compound increases with increasing polarity of the solvent. The energy differences between the gas phase and solvent media and dipole moments are shown in Fig. S10. As can be seen from Table S8, the dipole moments in the various solvents which are calculated using the SCI-PCM method increase with increasing solvent polarity. Optimization calculations at B3LYP/6-311++G(d,p) level were also performed for both the enol and keto forms of compound to investigate the tautomeric stability. In the gas phase, the total energy of the enol-imine form is lower than the keto-amine form.

3.8. Molecular electrostatic potential surface

To investigate reactive sites for electrophilic and nucleophilic attack, the regions of the MEP for the compound were investigated by DFT calculation using the optimized geometry of the B3LYP/6-311++G(d,p). As shown in Fig. S11, red and yellow colours indicate the negative regions of the MEP are related to electrophilic reactivity, while blue colours indicate positive regions related to nucleophilic reactivity. As can be seen from Fig. S11, the compound has one possible site for electrophilic attack. The oxygen atom O1 of the hydroxy group has a negative region. The maximum negative molecular electrostatic potential value is 0.025 a.u. for the main region of the O1 atom. The C7–H7, C9–H9, C11–H11, and C13–H13, bonds indicate a possible site for nucleophilic attack with a maximum value of 0.050 a.u. and around these bonds are maximum positive regions. According to these calculated results, the region of MEP shows that the negative potential sites are on electronegative atoms while the positive potential sites are around the hydrogen atoms. The determining of MEP region is best suited to identify sites for intra- and intermolecular interactions. According to the MEP surface of the compound, the weak negative region is

associated with O1 atom and also the weak positive region is around the nearby H1 atom. It can be indicative of an intramolecular (N1–H1···O1) hydrogen bonding in the compound.

3.9. Nonlinear optical (NLO) effects

To investigate the nonlinear optical properties of molecules is very important because of the key functions of frequency shifting, optical modulation, optical switching, optical logic and optical memory for emerging technologies in areas such as telecommunications, signal processing and optical interconnections [84]. Thanthiriwatte and Nalin de Silva have explained in detail previously how to calculate the total dipole moment (μ_{tot}), linear polarizability (α_{ij}), and the first-order hyperpolarizability (β_{ijk}) from the Gaussian output file [85].

The total molecular dipole moment (μ), linear polarizability (α), and the first-order hyperpolarizability (β) were calculated by the B3LYP method with each of the 6-31G(d), 6-31+G(d,p), 6-31++G(d,p), 6-311+G(d) and 6-311++G(d,p) basis sets to investigate the effect of basis sets on the NLO properties. The calculated values of μ_{tot} , α_{tot} and β_{tot} are listed in Table S8. From Table S8, it can be seen that the calculated values of the μ_{tot} , α_{tot} and β_{tot} slightly depend on the size of basis sets. The values of the μ_{tot} , α_{tot} and β_{tot} obtained with the 6-31G(d) basis set are smaller than those obtained with the large size basis sets. It was found that the results calculated for the basis sets from 6-31+G(d) to 6-311++G(d,p) have minor differences.

It can be seen from Table S8 that the calculated values of β_{tot} for the compound are greater than urea (the β_{tot} of urea is $0.373 \times 10^{-30} \text{ cm}^5/\text{esu}$ obtained by using B3LYP/6-31G(d) basis set). When it is compared with similar Schiff base compounds in the literature, the calculated values of β_{tot} for the compound are larger than that of (*E*)-*N*-{2-[2-hydroxybenzylidene)amino]-phenyl}benzenesulfonamide ($\beta_{tot} = 7.98 \times 10^{-30} \text{ cm}^5/\text{esu}$) [75], and 2-[2,4-dimethylphenyl]iminomethyl]-3,5-dimethoxyphenol ($\beta_{tot} = 8.256 \times 10^{-30} \text{ cm}^5/\text{esu}$) [76],

calculated with B3LYP/6-311++G(d,p) method. The calculated value of $\beta_{tot} = 8.55 \times 10^{-30}$ cm⁵/esu in the gas phase, which is greater than that of urea ($\beta_{tot} = 0.592 \times 10^{-30}$ cm⁵/esu obtained by using B3LYP/6-311++G(d,p) method). Especially, the first-hyperpolarizability value of the investigated compound is about 14 times more than that of urea at the same level B3LYP/6-311++G(d,p) base set.

3.10. Thermodynamic Properties

The heat capacity ($C_{p,m}^0$), entropy (S_m^0) and enthalpy (H_m^0) are the standard thermodynamic functions and were performed using the DFT/B3LYP method with 6-311++G(d,p). The results obtained from the vibrational analysis are shown in Table S9. The heat capacities, entropies and enthalpies were obtained by increasing temperature from 200 K to 450 K. As a result, the increase in temperature increases heat capacities, entropies and enthalpies due to increasing intensities of molecular vibration. The correlations between the thermodynamic properties $C_{p,m}^0$, entropy S_m^0 and enthalpy H_m^0 and temperatures T are described and shown in Fig. S12, according to the data in Table S9. The correlation equations between these thermodynamic properties and temperature T are as follows:

$$C_{p,m}^0 = -1.4358 + 0.2891T - 0.00017T^2 \quad (R^2=0.9999) \quad (7)$$

$$S_m^0 = 71.817 + 0.2914T - 0.00007T^2 \quad (R^2=1) \quad (8)$$

$$H_m^0 = -0.5314 + 0.014T + 0.00017T^2 \quad (R^2=1) \quad (9)$$

The values of $C_{p,m}^0$, S_m^0 and H_m^0 can easily be obtained at any temperature using these relationships and these results will be helpful for further studies of the compound.

3.11. Minimum Inhibitory Concentration (MIC)

MIC was evaluated by broth micro dilution test. A loop full of bacteria was inoculated in 100 mL of nutrient broth at 37 °C for 20 h in a test-tube shaker at 150 rev min⁻¹. The test compounds were prepared by dissolving in a mini-mal volume of DMSO and were serially diluted in Muel-ler-Hinton broth at concentrations in the range of 1-500 µg/mL. The 24-h

bacterial cultures were then transferred into 10 mL of the Muller-Hinton broth (control and test compounds) and incubated at 37 °C for 24 h. The growth of bacteria was determined by measuring the turbidity after 24 h. Thus, the MIC was generally read as the smallest concentration of the drug in the series that prevents the development of visible growth of the test organism. The data reported in Table 10 are the average data from three experiments.

The antimicrobial activity spectrum of the Schiff base varied greatly. It can be observed from Table 10 that the antimicrobial results of Schiff base have a high antifungal effect on *C. albicans* ATCC 60193 and *C. tropicalis* ATCC 13803, while the compound has a low effect on bacteria. Likewise, the compound has stronger antibacterial effect against *S. aureus* ATCC 25923, *E. faecalis* ATCC 29212, *E. coli* ATCC 35218, *P. aeruginosa* ATCC 254992 and *P. vulgaris* ATCC 13315 compared to *B. subtilis* ATCC 6633 and *E. coli* ATCC 25922. This compound differs significantly in its activity against tested microorganisms. This difference may be attributed to the fact that the cell wall in Gram-positive bacteria are of a single layer, whereas the Gram-negative cell wall is a multilayered structure, and the yeast cell wall is quite complex. Some *C. albicans* species have shown resistance to antifungal drugs [86].

3.12. DNA-Schiff base interaction studies

The potential binding ability of the Schiff base to CT-DNA was characterized by UV spectroscopy. The absorption spectra of Schiff base in the absence and presence of CT-DNA at different concentrations are given in Fig. 13. The absorption peaks at 278 nm and 310 nm are attributed to intraligand $\pi-\pi^*$ transition. With the concentration of CT-DNA increased, hyperchromism of 86.9%-133.5% and higher wavelength of 1-19 nm are observed at 278 nm, while hypochromism of 1.0%–46.0% and red shift of 1 nm are observed at 310 nm. In addition, the maximum absorption shifted to red indicates a decrease in energy between the HOMO and LUMO. This explains the interaction of DNA with a Schiff base [87]. Once the

DNA interacts with the Schiff base, π - π^* transition energy decreases, and the absorption shifts to red. Hypochromism, hyperchromism and bathochromism in UV absorption spectra, probably due to stacking interaction between an aromatic ring and the base pairs of DNA, suggest the Schiff base can interact with CT-DNA [27, 88, 89]. The extent of the hypochromism and hyperchromism are commonly consistent with the strength of intercalative and electrostatic interaction [27, 88, 89]. Surprisingly, the compound has both intercalative and electrostatic binding. Possible mechanisms are shown in Scheme 2 and 3. The Schiff base enters between the two amino acid molecules of the DNA in the intercalative binding (Scheme 2). In the electrostatic binding (Scheme 3), DNA breaks protons from the more acidic Schiff base. As a result, the negative charge distribution is changed in the DNA chain. Therefore, this leads to disruption of the DNA molecule.

3.13. Colorimetric anion-sensing

The binding ability of the sensor compound was firstly studied using UV-Vis spectral titrations in DMSO. Figure 14 shows spectral changes of the Schiff base in the absence and presence of hydroxy, fluoride, cyanide and acetate ions in DMSO solution. Upon the addition of 3 equiv of each anion, only OH^- , F^- , CN^- and AcO^- induced distinct spectral changes while the other anions did not induce any spectral changes (Fig. 14). As a result, the solution color of the compound changed from colorless to purple only with CN^- and to orange with F^- and AcO^- , and to yellow with OH^- with a fast response time, indicating that the receptor Schiff base ligand can serve as a “naked-eye” indicator for F^- , CN^- , AcO^- and OH^- in DMSO (Fig. 15).

The free Schiff base ligand shows absorption in the range less than 400 nm in DMSO. The presence of OH^- , F^- , CN^- and AcO^- resulted in absorbance bands greater than 400 nm decreasing gradually and new absorbance bands appeared at 435, 416, 416 and 422 nm, respectively. The excited-state intramolecular proton transfer [29-37] between hydroxy (-OH)

and nitrogen atom of imine ($-\text{C}=\text{N}-$) groups was inhibited and as a result, the emission band greater than 400 nm resulting from excited-state intramolecular proton transfer disappeared, inducing colorimetric changes to the compound. The high selectivity of the compound for hydroxy and fluoride may be due to the nucleophilicity of hydroxy and fluoride in DMSO. The order of selectivity or the binding affinity of anions for the Schiff base ligand is $\text{OH}^- > \text{F}^- > \text{CN}^- > \text{AcO}^- > \text{H}_2\text{PO}_4^- \sim \text{Br}^- \sim \text{I}^- \sim \text{SCN}^- \sim \text{ClO}_4^- \sim \text{HSO}_4^- \sim \text{N}_3^-$. The more acidic hydroxyl proton would deprotonate upon exposure to more basic OH^- , F^- and AcO^- ions and therefore, the intramolecular proton transfer occurs to the keto-amine form [90] (Scheme 4). In contrast, cyanide has much weaker hydrogen bonding ability in comparison with OH^- , F^- and AcO^- with stronger nucleophilicity toward the imine group, which results in the addition reaction of CN^- to the carbon atom of an electron deficient imine group and, subsequently, fast proton transfer of the phenol hydrogen to the neighboring nitrogen anion through an intramolecular hydrogen bond [91] (Scheme 5). The formation of the keto-amine form of the compound leads to higher wavelength absorption. The presence of other anions tested without similar basicity as OH^- , F^- , CN^- and AcO^- , such as Br^- , I^- , SCN^- , ClO_4^- , HSO_4^- , H_2PO_4^- and N_3^- , do not exhibit similar absorption.

3.14. $^1\text{H-NMR}$ spectral titrations

^1H NMR titrations were carried out in DMSO-d_6 (Fig. 16a, 16b, 16c). As can be seen in Fig. 16a, the free compound showed one peak at 12.25 ppm, which could be ascribed to -OH proton. When fluoride ions are mixed (0.5 equiv.), the -OH peak intensity decreases (Fig. 16b). When fluoride ions were introduced (1.0 equiv.), the signal at 12.25 ppm disappeared (Fig. 16c), indicating the -OH moiety of the compound acted as anion binding site and exhibited deprotonation upon interacting with strong basic anions. Therefore, the significant higher wavelength shifts in absorption and color changes resulted from

deprotonation of the anion binding sites [92]. Likewise, the ^1H NMR titrations of the compound with F^- also support the results obtained from the UV-Vis titrations.

4. Conclusions

(*E*)-2-[(3,5-bis(trifluoromethyl)phenylimino)methyl]phenol ($\text{C}_{15}\text{H}_7\text{F}_6\text{NO}$) was synthesized and characterized by spectroscopic method and X-ray single crystal diffraction. In addition, density functional modelling studies of the Schiff base ligand were reported in this study. Theoretical calculations were employed to determine the molecular structure, spectroscopic values, HOMOs, LUMOs levels of the compound. The theoretical calculations were found to be in good agreement with the experimental data. However, the DFT method seems to be more convenient than the HF method to calculate the bond angles and geometry of the investigated compound. In the compound, the X-ray single crystallographic study, NMR, FT-IR and DFT calculations revealed that the compound exists in the enol-imine form, which is mainly stabilized by the intramolecular $\text{O}-\text{H}\cdots\text{N}$ interactions. In addition to investigating the tautomeric stability of the compound, as seen from the calculations, the total energy of the enol form is lower than the keto-amine form which also reveals that the enol-imine tautomer is favored over the keto-amine tautomer. The total molecular energies obtained by the PCM method decrease with increasing polarity of the solvent and the stability of the compound increases in going from the gas phase to the solution phase. The MEP map shows that the negative potential sites are on electronegative atoms while positive potential sites are around the hydrogen atoms. These sites give intra and intermolecular interactions. In the compound, the weak negative region associated with N1 atom and also the weak positive region of the nearby H1 atom are indicative of intramolecular ($\text{O1}-\text{H1}\cdots\text{N1}$) hydrogen bonding. According to the calculated Mulliken atomic charges, the imine N1 atom has a large positive atomic charge and the hydroxyl O1 atom has a large negative atomic charge in the gas phase. This behavior may be the result of the $\text{N1}-\text{H}\cdots\text{O1}$ hydrogen bond. On the other

hand, the negative atomic charge values of the O atoms in the solution phase become more negative while the positive atomic charge of N1 decreases with the increase in the polarity of the solvent. The ab initio B3LYP calculations allow a more accurate prediction of the NLO activity for the compound. Our computational results yield that β_{tot} for the compound is greater than that of urea. The calculated values of β_{tot} of the investigated compound are also compared with the similar Schiff base compounds in the literature. So, the investigated compound is a good candidate as second-order NLO material. The thermodynamic properties, of $C_{p,m}^0$, S_m^0 , H_m^0 and temperatures T were also obtained. The results show that the standard thermodynamic functions increase at any temperature from 200 to 450 K, because the intensity of the molecular vibrations increase with increasing temperature.

The compound could act as real-time colorimetric sensor for anions. However, in this study, the compound was active against both types of bacteria and as well as active against yeasts, which may indicate broad-spectrum properties. DNA was affected in two ways by the compound. Electrostatic interaction was found to be very strong according to intercalative interaction.

We hope that the synthesis, crystallographic and spectroscopic characterization, DNA binding, anion sensing and DFT studies of the Schiff base (*E*)-2-[(3,5-bis(trifluoromethyl)phenylimino)methyl]phenol ($\text{C}_{15}\text{H}_7\text{F}_6\text{NO}$) will be helpful for the design and synthesis of new materials.

Acknowledgements

The authors are grateful to Ankara University Grants Commission for a research grant (Project No. : 2014H0430005) and Çanakkale Onsekiz Mart University Grants Commission for a research grant (Project No. : FDK-2015-307).

Appendix A. Supplementary material

Supplementary data associated with this article can be found, in the online version, at <http://dx.doi.org/>

References

- [1] K. Mounika, B. Anupama, J. Pragathi, C. Gyanakumari, *J. Sci. Res.* 3 (2010) 513-524.
- [2] P. Venkatesh, *Asian J. Pharma. Health Sci.* 1 (2011) 8-11.
- [3] M. Yıldız, B. Dülger, S.Y. Koyuncu, B.M. Yapıcı, *J. Ind. Chem. Soc.* 81(2004) 7-12.
- [4] H. Ünver, M. Yıldız, B. Dülger, Ö. Özgen, E. Kendi, T.N. Durlu, *J. Mol. Struct.* 737 (2005) 159-164.
- [5] M. Yıldız, H. Ünver, B. Dülger, D. Erdener, N. Ocak, A. Erdönmez, T.N. Durlu, *J. Mol. Struct.* 738 (2005) 253-260.
- [6] M. Yıldız, B. Dülger, A. Çınar, *J. Ind. Chem. Soc.* 82 (2005) 414-420.
- [7] M. Yıldız, A. Kiraz, B. Dülger, *J. Serb. Chem.* 72, 3 (2007) 215-224.
- [8] A. Kiraz, M. Yıldız, B. Dülger, *Asian J. Chem.* 21, 6 (2009) 4495-4507.
- [9] S.M. Sondhi, N. Singh, A. Kumar, O. Lozach, L. Meijer, *Bioorg. Med. Chem.* 14,11 (2006) 3758-3765.
- [10] A. Budakoti, M. Abid, A. Azam, *Eur. J. Med. Chem.* 41(2006) 63-70.
- [11] A. Pandey, D. Dewangan, S. Verma, A. Mishra, R. D. Dubey, *Int. J. Chem. Tech. Res.* 3 (2011) 178-184.
- [12] C. Chandramouli, M.R. Shivanand, T.B. Nayanbhai, B. Bheemachari, R.H. Udipi, *J. Chem. Pharm. Res.* 4, 2 (2012) 1151-1159.
- [13] R.P. Chinnasamy, R. Sundararajan, S. Govindaraj, *J. Advan. Pharm. Techno. Res.* 1, 3 (2010) 342-347.
- [14] A.K. Chaubey, S.N. Pandeya, *Int. J. Phar.Tech. Research.* 4 (4) 590 (2012)

- [15] T. Aboul-Fadl, F.A. Mohammed, E.A. Hassan, *Arch. Phar. Res.* 26, 10 (2003) 778-784.
- [16] R. Miri, N. Razzaghi-asl, M.K. Mohammadi, *J. Mol. Model.* 19, 2 (2013) 727-735.
- [17] S.M.M. Ali, M.A.K. Azad, M. Jesmin, S. Ahsan, M.M. Rahman, J.A. Khanam, M.N. Islam, S.M.S. Shahriar, *Asian Pacif. J. Trop. Biomed.* 2, 6 (2012) 438-442.
- [18] D. Wei, N. Li, G. Lu, K. Yao, *Sci. China B.* 49, 3 (2006) 225-229.
- [19] P.G. Avaji, C.H.V. Kumar, S.A. Patil, K.N. Shivananda, C. Nagaraju, *Eur. J. Med. Chem.* 44, 9 (2009) 3552-3559.
- [20] P.G. Cozzi, *Chem. Soc. Rev.* (2004) 410-421.
- [21] S. Chandra, *J. Sangeetika, J. Indian Chem. Soc.* 81, (2004) 203-206.
- [22] Z.H. Chohan, M. Praveen, A. Ghaffar, *Met. Based Drugs.* 4, 5 (1997) 267-272.
- [23] Z.H. Chohan, M. Arif, Z. Shafiq, M. Yaqub, C.T. Supuran, *J. Enzyme Inhib. Med. Chem.* 21 (2006) 95-103.
- [24] Y.P. Wang, Y.N. Xiao, C.X. Zhang, R.M. Wang, *J. Macromol. Sci. Part A*, 38 (2001) 1099-1104.
- [25] M.M. Ali, M. Jesmin, M.K. Sarker, M.S. Salahuddin, M.R. Habib, J.A. Khanam, *Int. J. Biol. Chem. Sci.* 2 (2008) 292-298.
- [26] B.S. Molla, B.S. Rao, K. Shridhara, P.M. Akberali, *Farmacology.* 55 (2000) 338-344.
- [27] X. Qiao, Z.Y. Ma, C.Z. Xie, F. Xue, Y.W. Zhang, J.Y. Xu, Z.Y. Qiang, J.S. Lou, G.J. Chen, S.P. Yan, *J. Inorg. Biochem.* 105 (2011) 728-737.
- [28] P. de Hoog, M.J. Louwerse, P. Gamez, M. Pitié, E.J. Baerends, B. Meunier, J. Reedijk, *Eur. J. Inorg. Chem.* (2008) 612-619.
- [29] S. Roy, P.U. Maheswari, M. Lutz, A.L. Spek, H. Dulk, S. Barends, G.P. van Wezel,

- F.Hartl, J. Reedijk, Dalton Trans. (2009) 10846-10860.
- [30] S. Dalapati, S. Jana, N. Guchhait, Spect. Acta Part A: Mol. Biomol. Spect. 129 (2014) 499-508.
- [31] K.S. Saravana, B. Shilpa, K.S. Suban, S.K.A. Kumar, J. Fluorine Chem. 164 (2014) 51-57.
- [32] D. Sharma, S.K. Ashok Kumar, S.K. Sahoo, Tetrahedron Lett. 55, 4 (2014) 927-930.
- [33] X. Huang, Y. He, Z. Chen, C. Hu, Chin. J. Chem. 27 (2009) 1526-1530.
- [34] R. Arabahmadia, S. Amania, Supramol. Chem. 26 (2014) 321-328.
- [35] Y. Li, H. Lin, Z. Cai, H. Lin, Mini-Rev. In Organic Chem. 8 (2011) 25-30.
- [36] Y.M. Hijji, B. Bararea, A.P. Kennedy, R. Butcherb, Sensors and Actuators B. 136 (2009) 297-302.
- [37] S. Devaraj, D. Saravanakumar, M. Kandaswamy, Tetrahedron Lett. 48, 17 (2007) 3077-3081.
- [38] M. Yıldız, Z. Kılıç, T. Hökelek, J. Mol. Struct. 441(1998) 1-10.
- [39] H. Nazır, M. Yıldız, H. Yılmaz, M.N. Tahir, D. Ülkü, J. Mol. Struct. 524 (2000) 241-250.
- [40] M. Yıldız, H. Ünver, D. Erdener, A. Kiraz, N.O. İskeleli, J. Mol. Struct. 919 (2009) 227-234.
- [41] H. Ünver, M. Yıldız, Spect. Lett. 43 (2010) 114-121.
- [42] H. Ünver, M. Yıldız, H. Özay, T.N. Durlu, Spectrochim. Acta Part A. 74 (2009) 1095-1099.
- [43] H. Özay, M. Yıldız, H. Ünver, N.O. İskeleli, Synt. React. Inorg., Met-Org., and Nano-Met.Chem. 42, 6 (2012) 872-877.
- [44] H. Ünver, M. Yıldız, A. Kiraz, N. Ocak, A. Erdönmez, B. Dülger, T.N. Durlu, J. Chem. Crystallogr. 36, 3 (2006) 229-237.

- [45] D. Amsterdam, Susceptibility testing of antimicrobials in liquid media. In: Antibiotics in laboratory medicine, Loman, V., ed., Williams and Wilkins, Baltimore, 1996, pp. 52-111.
- [46] I. Wiegand, K. Hilpert, R. E. W. Hancock, Nature Protocols. 3, 2 (2008) 163-175.
- [47] European committee for antimicrobial susceptibility testing (EUCAST) of the European society of clinical microbiology and infectious diseases (ESCMID). Determination of minimum inhibitory concentrations (MICs) of antibacterial agents by broth dilution, Clinical Microbiology and Infection, 9, 8 (2003) 1-7.
- [48] R.A. Miller, R.D. Walker, J. Carson, M. Coles, R. Coyne, I. Dalsgaard, C. Gieseke, H.M. Hsu, J.J. Mathers, M. Papapetropoulou, B. Petty, C. Teitzel, R. Reimschuessel, Dis. Aquat. Organ. 20, 64 (2005) 211-222.
- [49] Stoe & Cie, X-AREA (Version 1.18) and X-RED32 (Version 1.04) Stoe&Cie, Darmstadt, Germany, 2002.
- [50] G. M. Sheldrick, SHELXS-97, Program for the solution of crystal structures. Univ. of Goettingen, Germany, 1997.
- [51] G. M. Sheldrick, SHELXL-97, Program for the refinement of crystal structures. Univ. of Goettingen, Germany, 1997.
- [52] L. J. Farrugia, J. Appl. Crystallogr. 30 (1997) 565-565.
- [53] Further information may be obtained from: Cambridge Crystallographic Data Center (CCDC), 12 Union Road, Cambridge CB21EZ, UK, by quoting the depository number CCDC 1038662 E-mail: deposit@ccdc.cam.ac.uk.
- [54] F. Li, M. Feterl, Y. Mulyana, J.M. Warner, J.G. Collins, F.R. Keene, J. Antimicrob. Chemother. 67 (2012) 2686-2695.
- [55] J. Marmur, J. Mol. Biol. 3 (1961) 208-218.
- [56] M.J. Frisch, G.W. Trucks, H.B. Schlegel, G.E. Scuseria, M.A. Robb, J.R.

- Cheeseman, G. Scalmani, V. Barone, B. Mennucci, G.A. Petersson, H. Nakatsuji, M. Caricato, X. Li, H.P. Hratchian, A.F. Izmaylov, J. Bloino, G. Zheng, J.L. Sonnenberg, M. Hada, M. Ehara, K. Toyota, R. Fukuda, J. Hasegawa, M. Ishida, T. Nakajima, Y. Honda, O. Kitao, H. Nakai, T. Vreven, J.A. Montgomery, Jr.J.E. Peralta, F. Ogliaro, M. Bearpark, J.J. Heyd, E. Brothers, K.N. Kudin, V.N. Staroverov, R. Kobayashi, J. Normand, K. Raghavachari, A. Rendell, J.C. Burant, S.S. Iyengar, J. Tomasi, M. Cossi, N. Rega, J.M. Millam, M. Klene, J.E. Knox, J.B. Cross, V. Bakken, C. Adamo, J. Jaramillo, R. Gomperts, R.E. Stratmann, O. Yazyev, A.J. Austin, R. Cammi, C. Pomelli, J.W. Ochterski, R.L. Martin, K. Morokuma, V. G. Zakrzewski, G.A. Voth, P. Salvador, J.J. Dannenberg, S. Dapprich, A.D. Daniels, Ö. Farkas, J.B. Foresman, J.V. Ortiz, J. Cioslowski, D.J. Fox, Gaussian 09, Revision D.01 (Gaussian, Inc., Wallingford CT, 2009).
- [57] R. Dennington, T. Keith, J. Millam, GaussView, Version 5, Semichem, Inc., Shawnee Mission, KS, 2009.
- [58] A.D. Becke, *J. Chem. Phys.* 98 (1993) 5648-5652.
- [59] A.D. Becke, *J. Chem. Phys.* 104 (1996) 1040-1046.
- [60] G.A. Petersson, M.A. Al-Laham, *J. Chem. Phys.* 94 (1991) 6081-6090.
- [61] G.A. Petersson, A. Bennett, T.G. Tensfeldt, M.A. Al-Laham, W.A. Shirley, J. Mantzaris, *J. Chem. Phys.* 89 (1988) 2193-2218.
- [62] A.D. McLean, G.S. Chandler, *J. Chem. Phys.* 72 (1980) 5639-5648.
- [63] T. Clark, J. Chandrasekhar, G.W. Spitznagel, P.V.R. Schleyer, *Comp. Chem.* 4 (1983) 294-301.
- [64] P. Merric, D. Moran, I. Radom, *J. Phys. Chem. A* 111 (2007) 11683-11700.
- [65] G.Y. Yeap, S.T. Ha, N. Ishizawa, K. Suda, P.L. Boey, W.A.K. Mahmood, *J. Mol. Struct.* 658 (2003) 87-99.

- [66] B. Peng, G. Liu, L. Liu, D. Jia, K. Yu, J. Mol. Struct. 692 (2004) 217-222.
- [67] A. Bondi, J. Phys. Chem. 68 (1964) 441-451.
- [68] A. Teimouri, A.N. Chermahini, K. Taban, H.A. Dabbagh, Spectrochim. Acta A 72 (2009) 369-377.
- [69] H. A Dabbagh, A. Teimouri, A.N. Chermahini, M. Shahraki, Spectrochim. Acta A. 69 (2008) 449-459.
- [70] Ö. Tamer, N. Dege, G. Demirtaş, D. Avcı, Y. Atalay, M. Macit, S. Şahin, J. Mol. Struct. 1063 (2014) 295-306.
- [71] C. Arunagiri, A. Subashini , M. Saranya , P. Thomas Muthiah , K. Thanigaimani, I. Abdul Razak, Spectrochim. Acta. Part A 135 (2015) 307-316.
- [72] Y. Wang, Z. Yu, Y. Sun, Y. Wang, L. Lu, Spectrochim. Acta A 79 (2011) 1475-1482.
- [73] C.T. Zeyrek, N. Dilek, M. Yıldız, H. Ünver, Mol. Phys. 112, 19 (2014) 2557-2574.
- [74] A. Teimouri, A.N. Chermahini, K. Taban, H.A. Dabbagh, Spectrochim. Acta A 72 (2009) 369-377.
- [75] Y. Erdogan, M. Tahir Gulluoglu, Spectrochim. Acta A 74 (2009) 162-167.
- [76] N. Sundaraganesan, B.D. Joshua, K. Sethu, Spectrochim. Acta A 66 (2007) 381-388.
- [77] R.M. Silverstein, F.X. Webster, Spectroscopic identification of organic compounds, sixth ed., John wiley & Sons Inc. New York, 2003.
- [78] C.T. Zeyrek, H. Ünver, Ö.T. Arpacı, K. Polat, N.O. İskeleli, M. Yıldız, J. Mol. Struct. 1081 (2015) 22-37.
- [79] M. Govindarajan, K. Ganasan, S Periandy, S. Mohan, Spectrochim. Acta A76 (2010) 12-21.
- [80] A.R. Berenji, S.F. Tayyari, M. Rahimizadeh, H. Eshghi, M. Vakili, A. Shiri, Spectrochim. Acta Part A 102 (2013) 350-357.

- [81] R.M. Silverstein, F.X. Webster, Spectroscopic identification of organic compound, 6th ed., John Willey & Sons, New York, 1998.
- [82] I. Fleming, Frontier orbitals and organic chemical reactions, John Wiley and Sons, New York, 1976.
- [83] T. Koopmans, *Physica*, 1 (1933) 104-113.
- [84] C. Andraud, T. Brotin, C. Garcia, F. Pelle, P. Goldner, B. Bigot, A. Collet, *J. Am. Chem. Soc.* 116 (1994) 2094-2102.
- [85] K.S. Thanthiriwatte, K.M.N. de Silva, *J. Mol. Struct. (Theochem)*, 617 (2002) 169-175.
- [86] C.T. White, S. Holleman, F. Dy, F.L. Mirels, A.D. Stevens, *Antimicrob. Agents Chemother.* 46 (2002) 1704-1713.
- [87] F. Arjmand, M. Aziz, *Eur. J. Med. Chem.* 44, 2 (2009) 834-844.
- [88] G. Dehghan, J.E.N. Dolatabadi, A. Jouyban, K.A. Zeynali, S.M. Ahmadi, S. Kashanian, *DNA Cell Biol.* 30 (2011) 195-201.
- [89] C. Hiort, P. Lincoln, B. Norden, *J. Am. Chem. Soc.* 115 (1993) 3448-3454.
- [90] M. Yıldız, *Spect. Lett.* 37, 4 (2004) 367-381.
- [91] J.Y. Noh, I.H. Hwang, H. Kim, E.J. Song, K.B. Kim, C. Kim, *Bull. Korean Chem. Soc.* 34, 7 (2013) 1985-1989.
- [92] G. Baggi, M. Boiocchi, L. Fabbrizzi, L. Mosca, *Chem. Eur. J.* 17 (2011) 9423-9439.

Schemes, Figures and Tables Captions

Scheme 1. The chemical formula of the title compound.

Scheme 2. Intercalative binding between DNA and the compound.

Scheme 3. Electrostatic binding between DNA and the compound.

Scheme 4. The proposed sensing mechanism of the compound for OH^- , F^- and AcO^- anions in DMSO.

Scheme 5. The proposed sensing mechanism of the compound for CN^- anion in DMSO.

Fig. 1. ORTEP-3 [52] drawing of the compound with displacement ellipsoids plotted at 50% probability level; intramolecular hydrogen bonds are represented by dashed lines.

Fig. S2a. The calculated and experimental values of bond distances of the compound.

Fig. S2b. The calculated and experimental values of bond angles of the compound.

Fig. S2c. The calculated and experimental values of torsion angles of the compound.

Fig. S3a. Potential energy curve calculated at B3LYP/6-311++G(d,p) level for the investigated molecule along the T1(C9–C8–N1–C7) torsional angle.

Fig. S3b. Potential energy curve calculated at B3LYP/6-311++G(d,p) level for the investigated molecule along the T2(C1–C6–C7–N1) torsional angle.

Fig. 4. FT-IR Spectrum of the compound.

Fig. S5a. Correlation graphics of experimental and unscaled (calculated) frequencies of the compound.

Fig. S5b. Correlation graphics of experimental and scaled (calculated) frequencies of the compound.

Fig. S6. ^{13}C - NMR spectrum of the compound.

Fig. S7. UV-visible spectrum of the compound in DMSO solvent.

Fig. S8. HOMO-LUMO transitions.

Fig. S9. The Mulliken atomic charges for the excluded H atoms of the compound in gas phase.

Fig. S10. The energy difference between the gas phase and solvent media and dipole moments.

Fig. S11. Molecular electrostatic potential (MEP) map calculated at 6-311++G(d,p) level.

Fig. S12. Correlation graphics of thermodynamic properties and temperatures of the compound.

Fig. 13. Absorption spectra of compound in the absence and presence of increasing amounts of CT-DNA at room temperature in Tris–HCl/NaCl buffer (pH 7.2).

Fig. 14. Absorption spectra changes of compound (1equiv) upon addition of various anions (1 equiv) of the compound.

Fig. 15. The color changes of the compound (1equiv) upon addition of various anions (1 equiv) of the compound.

Fig. 16. $^1\text{H-NMR}$ Titration spectrum of the compound. **a)** 0.0 eq F^- , **b)** 0,5 eq F^- , **c)** 1.0 eq F^- .

Table S1. Crystal and experimental data.

Table S2. The experimental and optimized (HF, B1B95 and B3LYP/gas phase) with 6-311++G(d,p) level geometric parameters of the compound Bond distances (\AA) and angles ($^\circ$) with estimated standard deviations (e.s.d.s) in parentheses.

Table S3. Comparison of the experimental and calculated vibrational frequencies (cm^{-1})

Table 4. The calculated and experimental $^1\text{H-}$ and $^{13}\text{C-NMR}$ isotropic chemical shifts of the compound.

Table S5. Experimental and theoretical electronic absorption wavelength, oscillator strength, major contributions of calculated transitions for compound.

Table S6. Calculated total energies and dipole moments of the compounds in different solvents at B3LYP/6-311++G(d,p) level using the SCI-PCM method in gas phase.

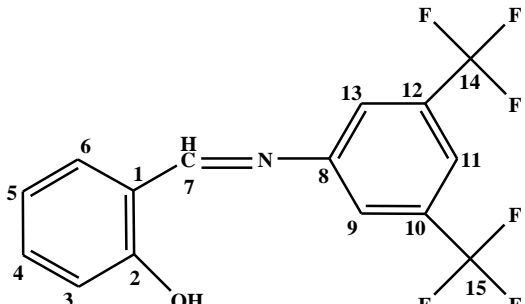
Table S7. Atomic charges (e) of the compound in gas phase and solution phase at the DFT with the functional B3LYP and B1B95 using the 6-311++G(d,p) basis set.

Table S8. Total dipole moment (μ), polarizability (α), and first hyperpolarizability (β) of the compound at B3LYP method.

Table S9. Thermodynamic parameters of the compound. Heat capacity ($C_{p,m}^o$), entropy (S_m^o) and enthalpy (H_m^o) based on the vibrational analysis at different temperatures at the DFT with the functional B3LYP using the 6-311++G(d,p) basis set.

Table 10. MIC ($\mu\text{g/mL}$) of the compound.

Table 4

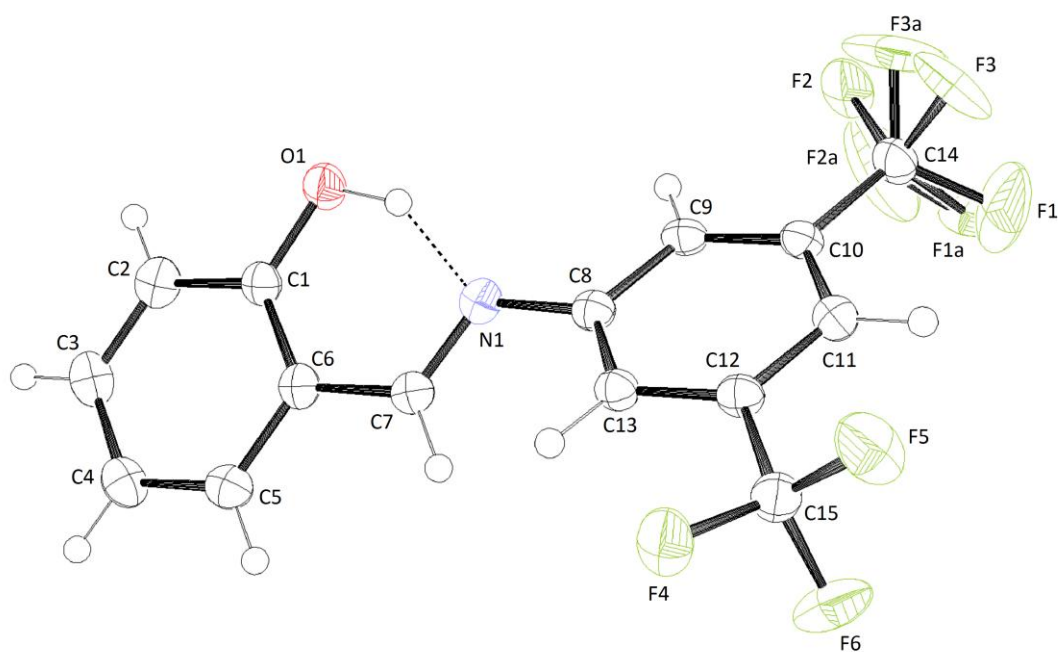


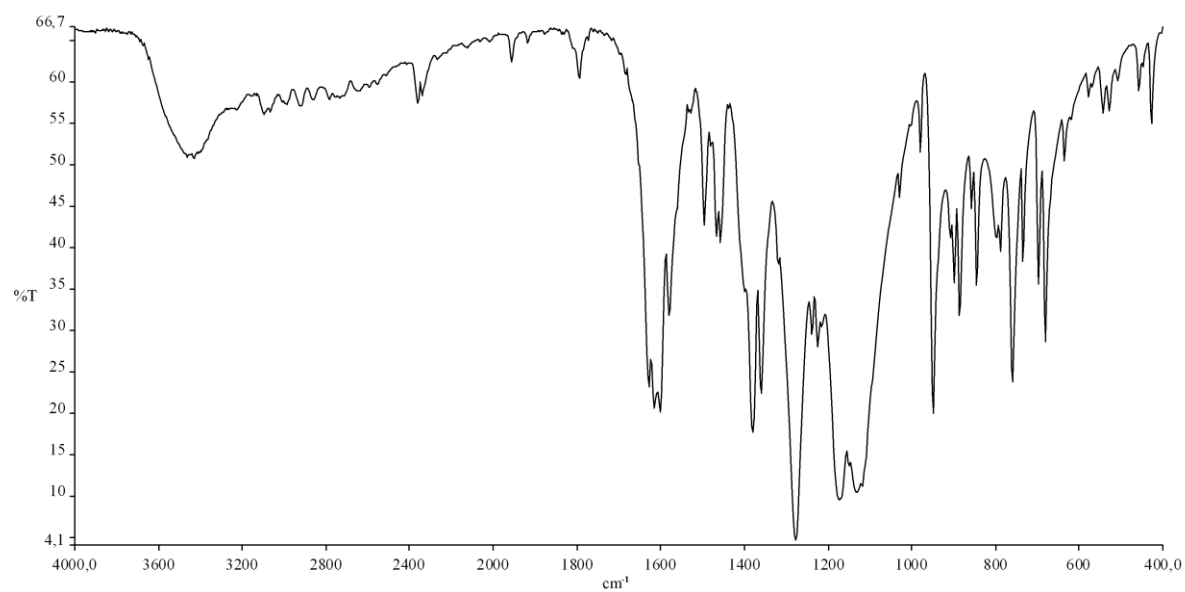
Nucleus	Exp. chemical shifts (ppm) (in DMSO-d6)	Cal. chemical shifts (ppm) (in gas)	Cal. chemical shifts (ppm) (in DMSO)	Nucleus	Exp. chemical shifts (ppm) (in DMSO-d6)	Cal. chemical shifts (ppm) (in gas)	Cal. chemical shifts (ppm) (in DMSO)
H(-O)	12.25	12.26	12.33	C1	119.89	123.44	123.76
H3	6.97	7.21	7.23	C2	160.23	170.71	169.48
H4	7.70	7.60	7.76	C3	116.73	122.31	121.14
H5	7.46	6.95	7.14	C4	132.71	140.58	140.88
H6	7.71	7.40	7.72	C5	122.07	122.89	123.70
H7	9.07	8.61	8.84	C6	131.48	137.84	139.42
H9	7.95	7.82	7.94	C7	166.57	169.64	172.07
H11	8.10	7.90	7.96	C8	150.62	158.00	158.16
H13	7.95	7.49	7.76	C9	124.24	130.61	131.41
				C10	134.35	139.28	137.78
				C11	122.48	125.36	125.30
				C12	134.35	139.82	138.72
				C13	124.24	121.82	123.84
				C14	131.21	133.19	133.58
				C15	131.21	133.24	133.69

Table 10

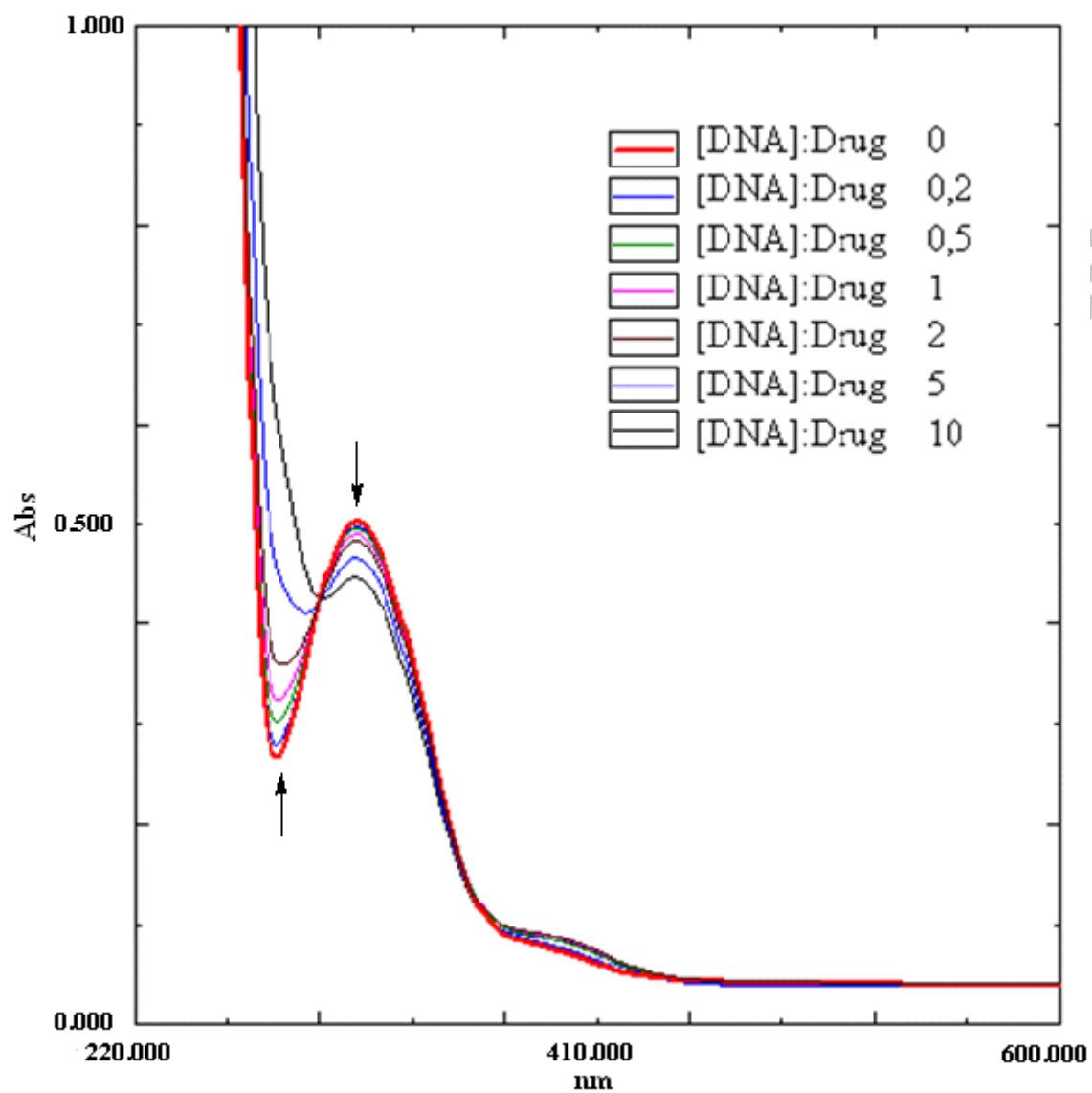
Microorganisms	Compound	Antibiotic		
		Gentamicin	Ampicillin	Fluconazol
<i>S. aureus</i> ATCC 25923	64	1	0.06	-
<i>E. faecalis</i> ATCC 29212	64	0.5	1	-
<i>B. cereus</i> NRRL B-3711	64	0.25	0.25	-
<i>B. subtilis</i> ATCC 6633	32	0.06	0.06	-
<i>E. coli</i> ATCC 25922	128	0.13	16	-
<i>E. coli</i> ATCC 35218	64	0.13	32	-
<i>P. aeruginosa</i> ATCC 254992	64	0.06	2	-
<i>P. vulgaris</i> ATCC 13315	64	0.13	0.06	-
<i>C. albicans</i> ATCC 60193	32	-	-	0.0625
<i>C. tropicalis</i> ATCC 13803	32	-	-	0.5

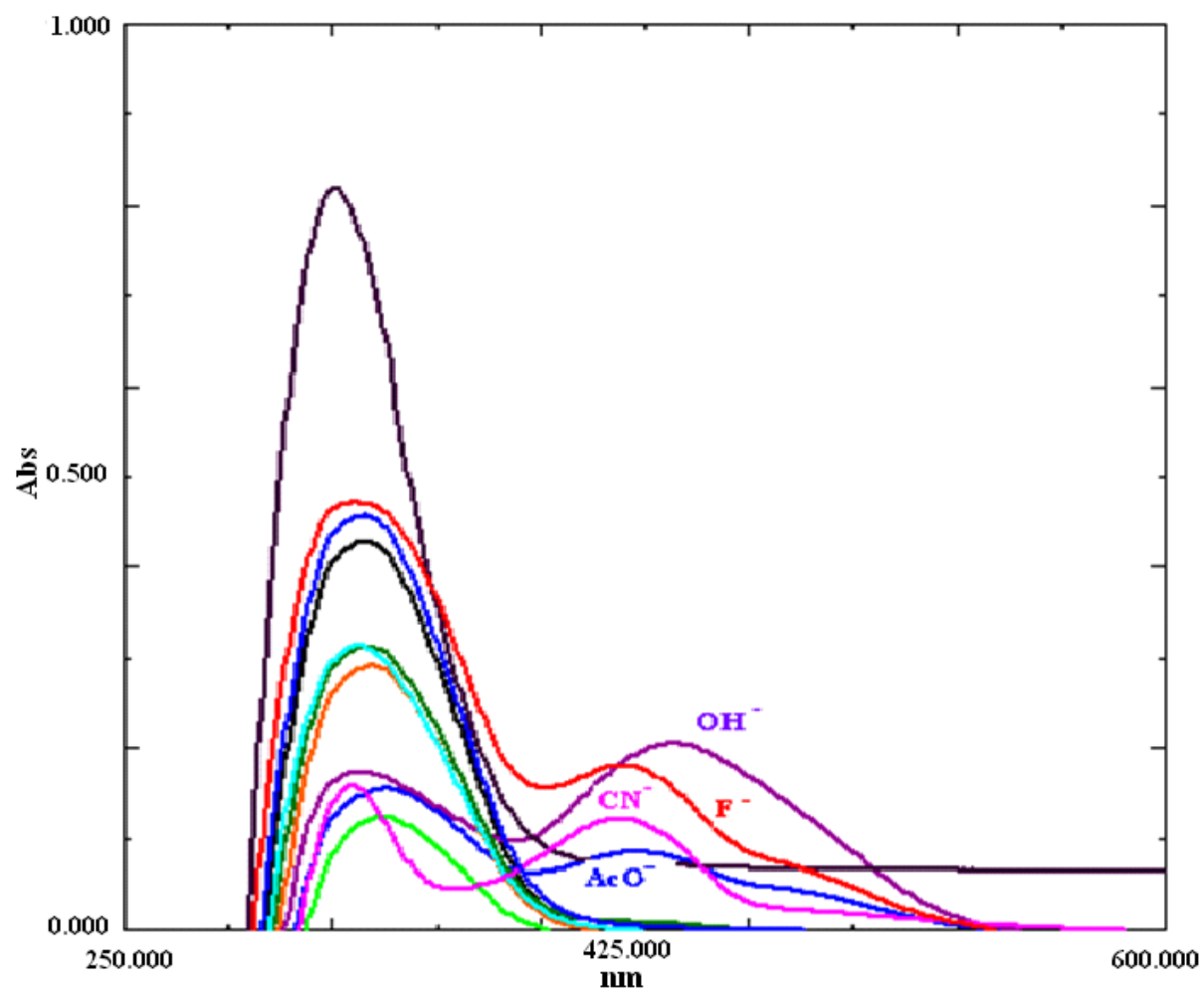
ACCEPTED MANUSCRIPT

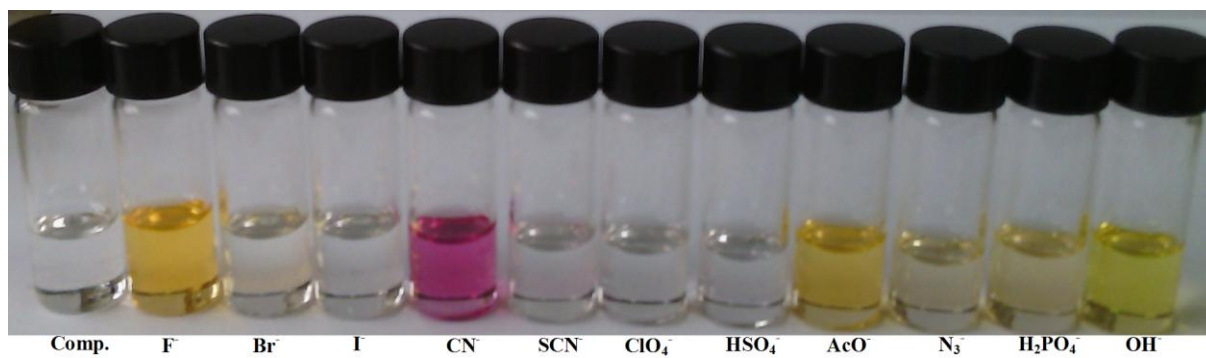




ACCEPTED MANUSCRIPT



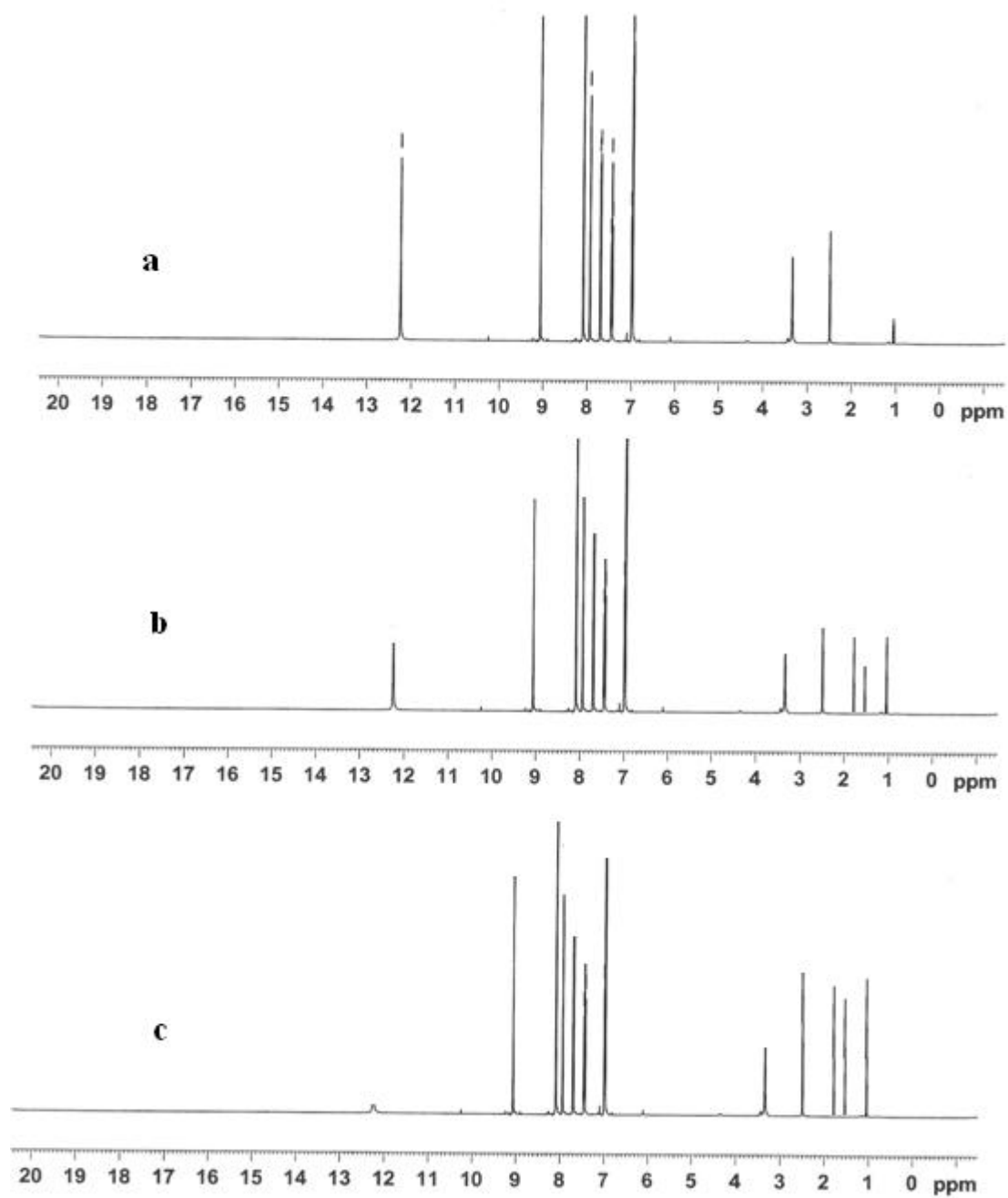




Comp.

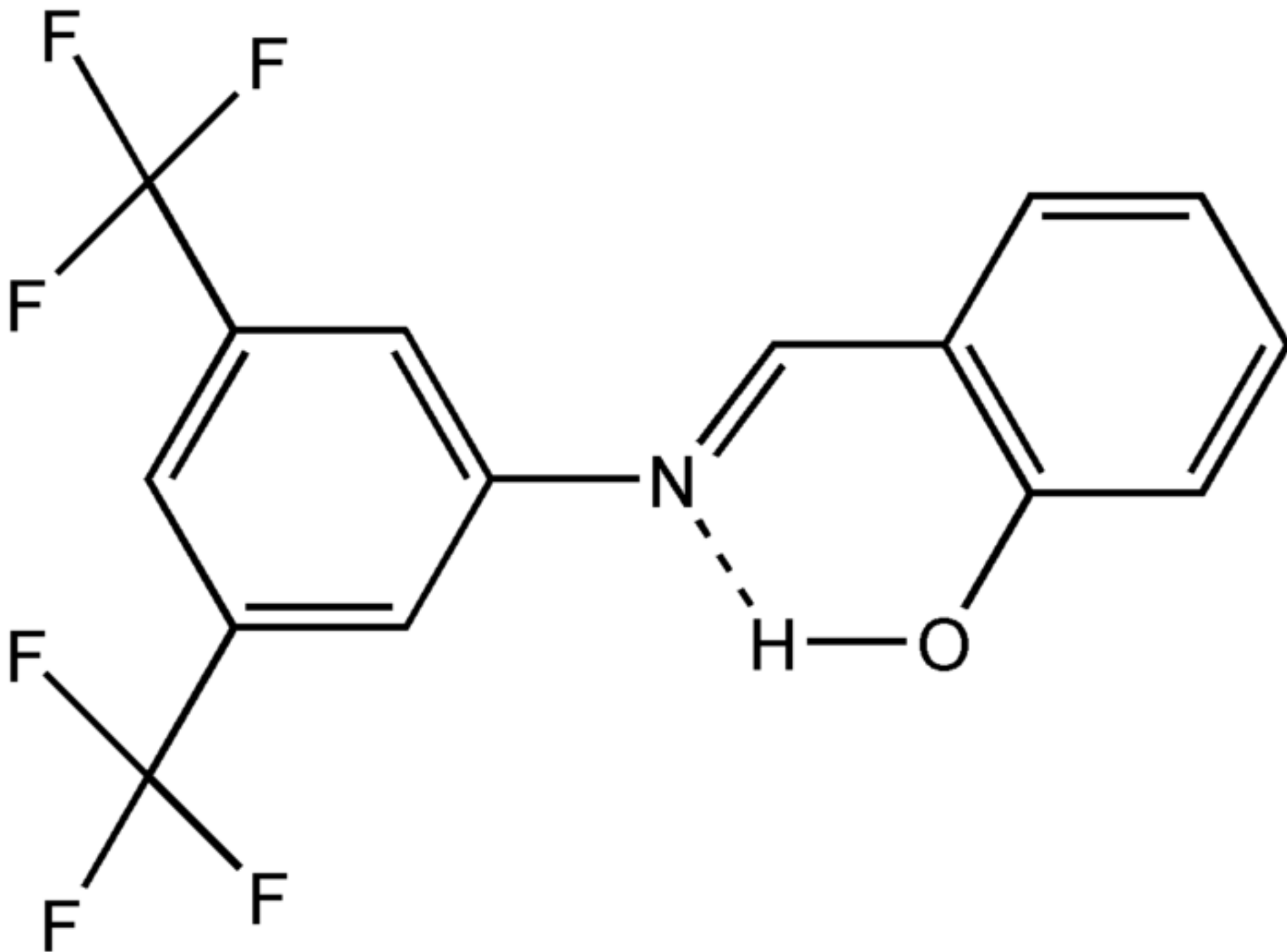
F⁻Br⁻I⁻CN⁻SCN⁻ClO₄⁻HSO₄⁻AcO⁻N₃⁻H₂PO₄⁻OH⁻

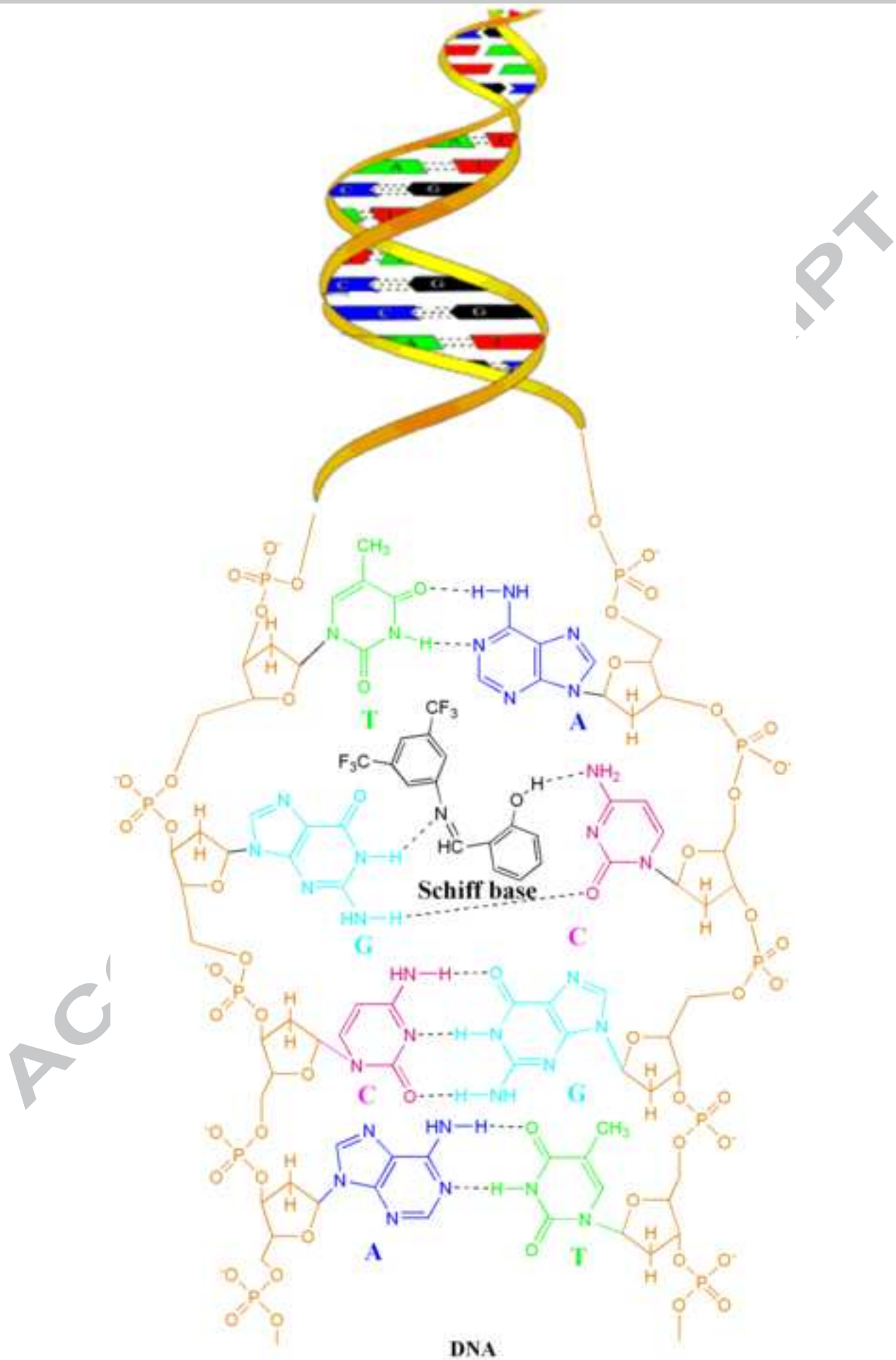
ACCEPTED MANUSCRIPT

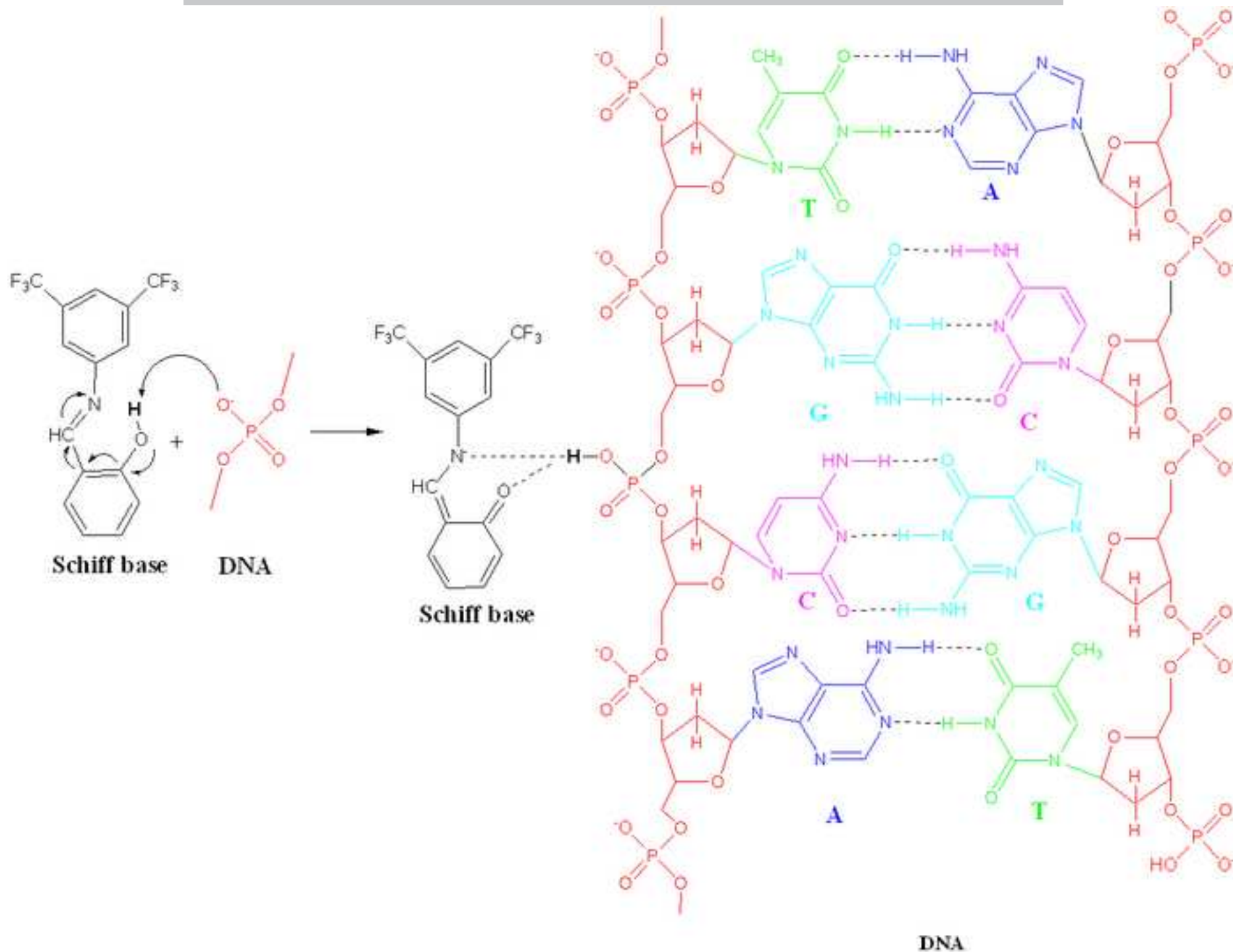


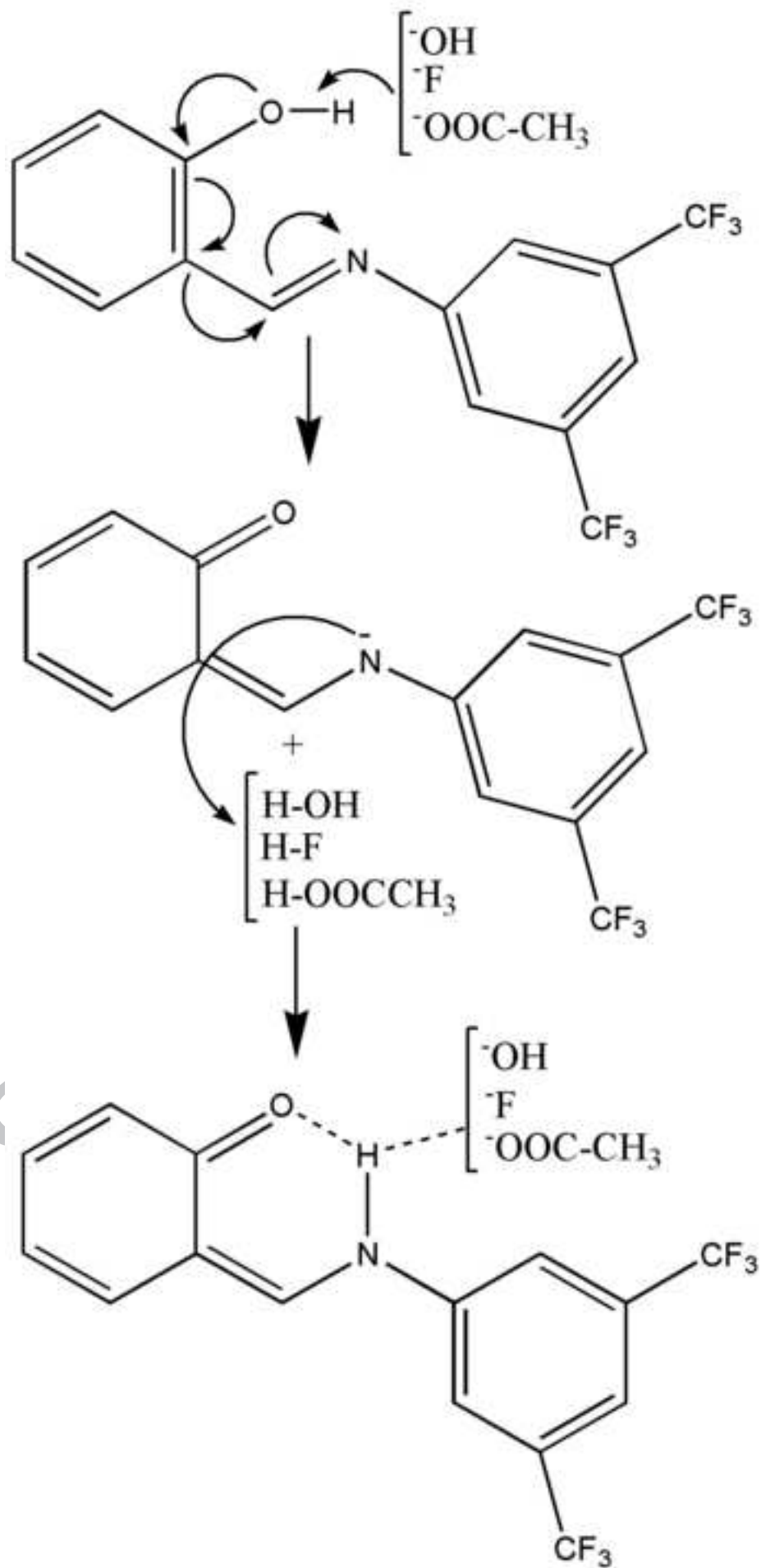
AC

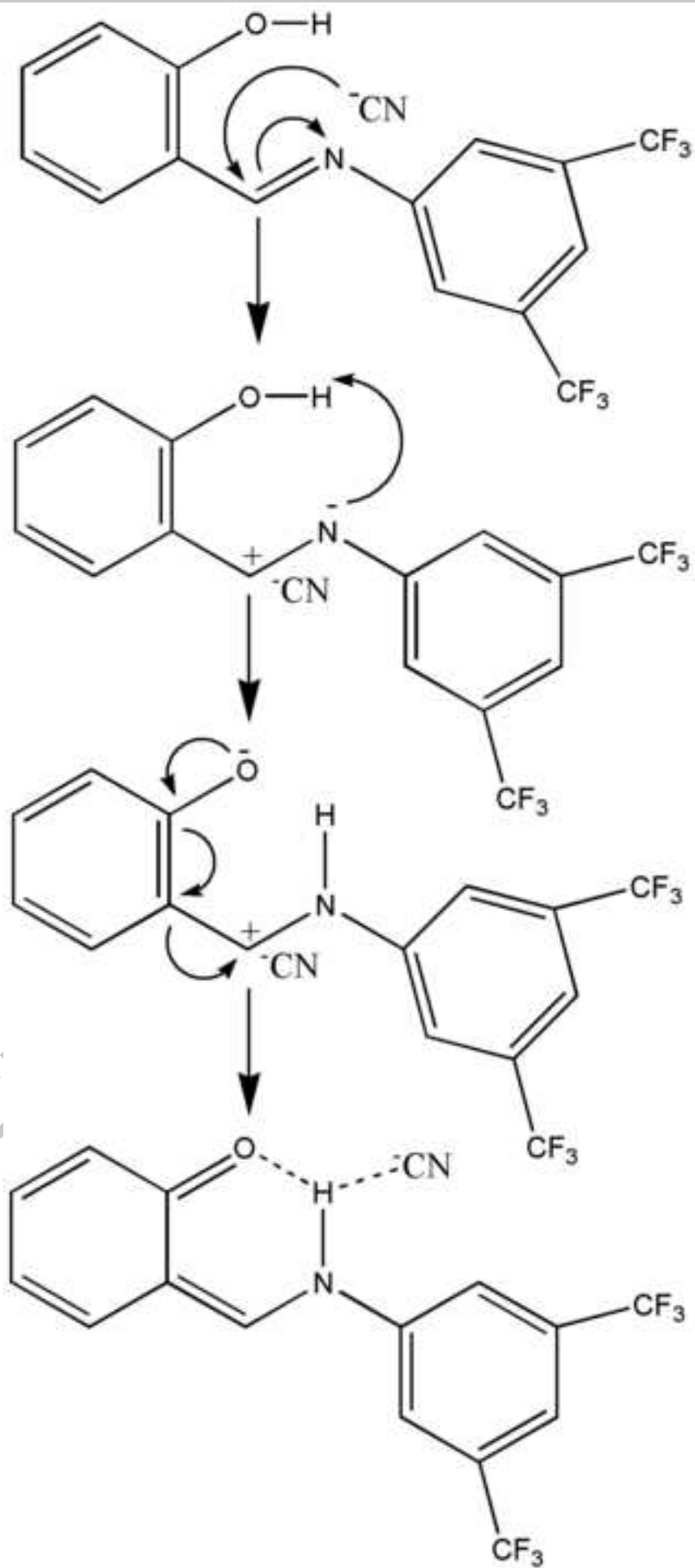
PT







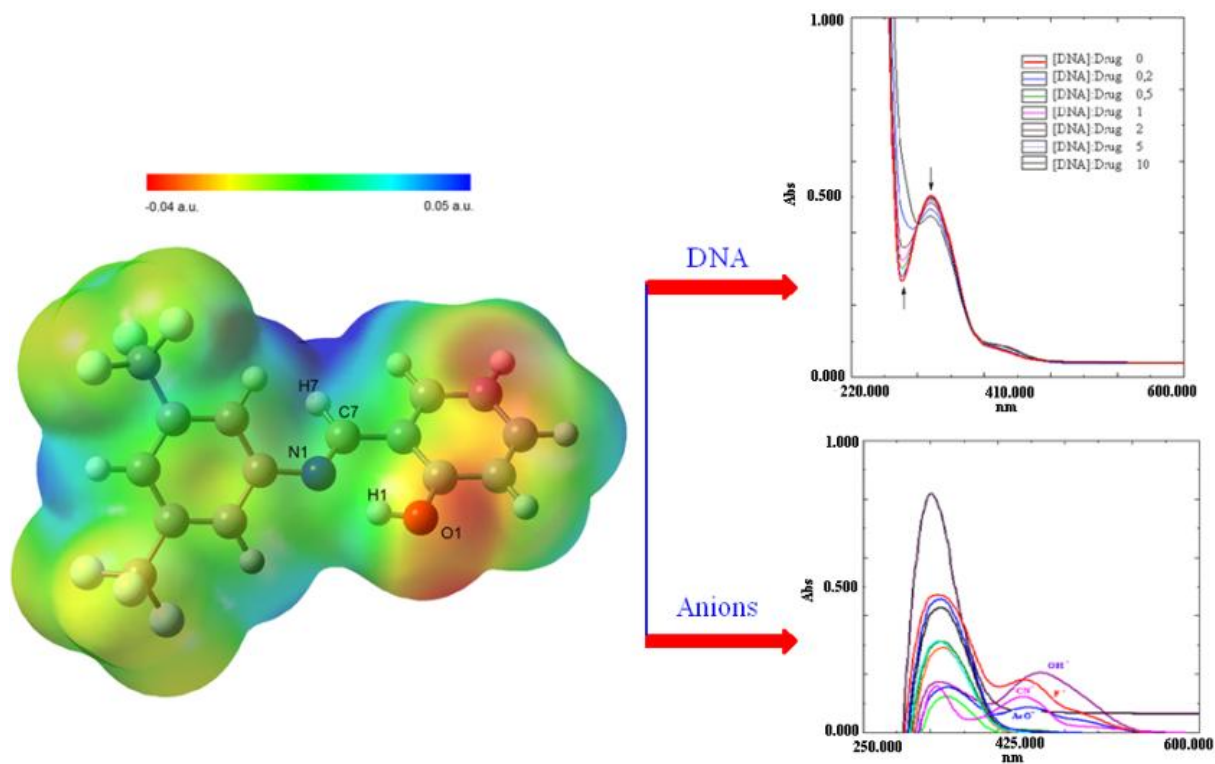




RIPT

ACC

Graphical abstract



ACCEPTED

Highlights

- The molecular structure of the compound in the ground state was studied.
- The potential binding ability of Schiff base to CT-DNA was characterized.
- The antimicrobial activities of the compound were investigated.
- The colorimetric response of the Schiff base receptors in DMSO was investigated.
- ^1H NMR titrations were carried out in DMSO-d_6 .

ACCEPTED MANUSCRIPT